International Journal of Thermal Sciences 223 (2026) 110586

Contents lists available at ScienceDirect

International Journal of Thermal Sciences

journal homepage: www.elsevier.com/locate/ijts

The influence of Prandtl number on the thermohydraulic behaviour of laminar mixed convective flow through horizontal tubes heated at a constant heat flux

Marilize Everts [a,b,*], Oluwasegun S. Omosehin [b], Wilhelm J. van den Bergh [b]

[a] Department of Mechanical Engineering, University College London, London, United Kingdom
[b] Department of Mechanical and Aeronautical Engineering, University of Pretoria, South Africa

ARTICLE INFO

Keywords:
Mixed convection
High Prandtl number
Constant heat flux
Thermal boundary layer
Hydrodynamic boundary layer

ABSTRACT

The influence of Prandtl number on laminar mixed convective flow through a smooth, horizontal tube was investigated using ANSYS Fluent 22 to improve the understanding of the interaction between buoyancy and fluid viscosity on the thermohydraulic behaviour. Different propylene glycol concentrations (0%, 30%, 50%, 70%, 80%, and 90%) were considered for heat fluxes of 200-10 000 W/m^2 and Reynolds numbers of 250-2000. The tube had an inner diameter of 5.1 mm and a length of 10 m. It was found that as the Prandtl number increased, the buoyancy force increased up to 74% for the 90% propylene glycol concentration compared to pure water, resulting in higher vorticity and circulation strength. However, this was confined near the tube wall and when quantifying the buoyancy effects using the secondary flow strength, viscosity-induced damping was found to decrease buoyancy effects by up to 95%. Conversely, for low-Prandtl number mixtures such as 0% and 30% propylene glycol concentrations, increased secondary flow thinned the thermal boundary layer and enhanced heat transfer by 40% and 28%, respectively, compared to forced convective flow, despite a lower buoyancy force. Furthermore, secondary flow strength was quantified and grouped into three distinct regions: (1) developing region, (2) suppression region, and (3) enhancement region. When viscous effects dominated at higher Prandtl numbers (70% and 90%), the velocity profile became skewed above the tube's centre, and the merging position of the hydrodynamic boundary layers shifted upwards, which is the opposite of the trend seen in fluids with lower Prandtl number (0%, and 30%). Furthermore, as the Prandtl number increased, the hydrodynamic boundary layers along the axis merge closer to the tube inlet, while the thermal boundary layers merge further downstream.

1. Introduction

Several studies have been conducted on forced convective flow through tubes [1–5], providing fundamental insights into how fluids flow and transfer heat under the influence of externally applied forces. However, forced convection conditions rarely occur in practical applications. Instead, a combination of forced and free convective flows, referred to as mixed convection, is commonly encountered in engineering systems. Examples include heat exchangers in HVAC systems, solar energy systems, nuclear reactors, and aerospace applications. Consequently, the study of mixed convection is essential for maximizing energy efficiency and the performance of these systems. Given the diversity of applications, these systems utilise different working fluids, each with distinct thermal and flow characteristics.

Research on mixed convective heat transfer has explored a range of working fluids, including low Prandtl number fluids ($0.7 < Pr < 7$), such as air and water, medium Prandtl number fluids ($10 < Pr < 28$), such as molten salts, and high Prandtl number fluids ($Pr > 30$), such as glycol mixtures and nanofluids. Among the earliest investigations, Mori et al. [6] experimentally studied the effect of buoyancy on airflow within a uniformly heated horizontal tube. Their findings revealed that the product of the Reynolds and Rayleigh numbers ($ReRa$) could be used to investigate the velocity and temperature distributions as well as buoyancy effects. They reported that buoyancy effects began to influence the local Nusselt number at approximately $ReRa = 10^3$ and were able to nearly double the Nusselt number compared to cases without secondary flow. McComas and Eckert [7] studied mixed convective laminar flow of

* Corresponding author. Department of Mechanical Engineering, University College London, London, United Kingdom.
E-mail address: m.everts@ucl.ac.uk (M. Everts).

https://doi.org/10.1016/j.ijthermalsci.2025.110586
Received 15 August 2025; Received in revised form 16 October 2025; Accepted 8 December 2025
Available online 17 December 2025

Nomenclature

A	Area [m^2]
BF	Buoyancy force [N/m^3]
C_p	Specific heat capacity [J/kg. K]
D	Inner diameter [m]
f	Friction factor [−]
F	Body force [N]
g	Gravitational acceleration [m/s^2]
Gr	Grashof number [−]
Gz	Graetz number [−]
h	Heat transfer coefficient [W/m^2. K]
j	Colburn j-factor [−]
k	Thermal conductivity [W/m. K]
L	Tube length [m]
n	Number of elements [−]
Nu	Nusselt number [−]
p	Perimeter [m]
P	Pressure [Pa]
Pr	Prandtl number [−]
$\dot{q}$	Heat flux [W/m^2]
Re	Reynolds number [−]
Ra	Rayleigh number [−]
t	Tube thickness [m]
T	Temperature [K]
u, v, w	Velocity component in x, y, and z-directions [m/s]
V	Local fluid velocity [m/s]
x, y	Cross-sectional positions [m]
z	Axial position along tube length [m]

Greek symbols

Γ	Circulation strength [m^2/s]
μ	Dynamic viscosity [kg/m. s]
ρ	Density [kg/m^3]
ρ_o	Density at reference temperature [kg/m^3]
ψ	Secondary flow strength [−]
β	Thermal expansion coefficient [1/K]
ν	Kinematic viscosity [m2/s]
ω	Vorticity [1/s]

Subscripts

f	Fluid
i	Inlet
m	Mean
o	Outlet
w	Wall

air through a uniformly heated horizontal tube for a Reynolds number range of 100–900. Buoyancy effects were found to be more pronounced at low Reynolds numbers and required a longer thermal entrance length. However, the study conducted by Bergles and Simonds [8], using water as the working fluid, found that the thermal entrance length decreased with increasing buoyancy effects.

The effect of tube inclination on mixed convective laminar heat transfer was also experimentally investigated using low Prandtl number fluids such as air and water. For instance, Mohammed and Salman [9] investigated a short inclined tube, with a length to diameter ratio of 30, heated at constant heat fluxes ranging from 60 to 400 W/m^2. Air with a Prandtl number of 0.7 was used and the Reynolds number ranged from 400 to 1600. They found that the surface temperature decreased as the inclination angle varied from 90° (vertical) to 0° (horizontal), particularly when free convection dominated. Similarly, Barozzi et al. [10] used water with a Prandtl number of 6.7 and a tube with a length to diameter ratio of 250. It was found that increasing the inclination angle from 0° to 60° reduced the heat transfer coefficients. Meyer et al. [11] also used water, but a much longer length to diameter ratio of 824.7. Heat transfer and pressure drop experiments were conducted for heat fluxes of 4000 and 8000 W/m^2 and Reynolds numbers ranging from 1000 to 6000 while the tube was inclined from -90^o to $+90^o$. Buoyancy effects diminished with increasing inclination (thus approaching vertical upward or downward flow), resulting in decreased laminar heat transfer coefficients and friction factors.

Most studies have focused on relatively short horizontal tubes (length to diameter ratios less than 250), which often fail to capture the full extent of the thermal entrance region. To address this, Meyer and Everts [12] used longer tubes with length to diameter ratios of 872 and 1373 to experimentally investigate mixed convective developing and fully developed flow. Using water with a Prandtl number of 6.9 as the working fluid and Reynolds numbers ranging from 500 to 10 000, they identified three distinct local laminar heat transfer regions: forced convection developing (FCD), mixed convection developing (MCD), and fully developed (FD). Their findings also highlighted that longer thermal entrance lengths are required for simultaneously developing hydrodynamic and thermal flows compared to hydrodynamically fully developed and thermally developing flows. A follow-up numerical study [13] further analysed the concurrent development of hydrodynamic and thermal boundary layers in laminar mixed convective flows and refined the entrance region to consist of six distinct regions.

Apart from circular tubes, numerical studies also investigated mixed convective laminar flow through non-circular channels using low Prandtl number fluids. Chen et al. [14] considered water as the working fluid with various hydraulic diameters (4 mm, 8 mm, and 11.5 mm) and aspect ratios (0.5, 1, and 2). Their findings highlighted that the Nusselt number increased as the hydraulic diameter increased and aspect ratio decreased due to the formation of a secondary vortex pair. Chong et al. [15] considered mixed convective flow in a rectangular tube and found that the local Nusselt number at the bottom wall was highest, due to the influence of secondary flow, while the top wall exhibited the lowest Nusselt number. Furthermore, the Nusselt number increased with Reynolds number and Grashof numbers up to a limit of $Re = 1\,500$, beyond which the Nusselt number became independent of the Grashof number.

For circular tubes, both horizontal and vertical, studies have extended beyond conventional fluids such as water and air to liquid metals and specific nanofluids to include lower Prandtl numbers. Mansour et al. [16] numerically studied laminar mixed convective flow of a water-based alumina nanofluid (water-Al_2O_3) through an inclined tube heated at a uniform heat flux. Similar to Akbari et al. [17], the addition of nanoparticles effectively enhanced secondary flow in the developing region. Also using water-based alumina nanofluids, Mansour et al. [18] considered inclined tubes and found that increasing the particle concentration in the base fluid decreased the Nusselt number due to increased fluid dynamic viscosity, especially when the tube was horizontally oriented. Colla et al. [19] used TiO_2-water nanofluids (Prandtl numbers ranging from 6.7 to 6.9) and reported a delay in the onset of free convection due to Brownian motion and thermophoretic diffusion, which is consistent with the findings of Buongiorno et al. [20] and Yang et al. [21]. Using liquid metals (sodium and mercury with Prandtl numbers less than 0.1), Wang et al. [22] numerically investigated the concurrent buoyancy effect and axial conduction of laminar flow through horizontal and vertical tubes. For horizontal tubes, a reverse velocity flow was observed at the upper part of the tube as free convection became significant. The location of reverse flow shifted upstream as the Prandtl number decreased.

Focussing on medium Prandtl number fluids, Zhang et al. [23] used molten salts (Pr = 4.4 to 28) and found that the onset of mixed

convective flow and thermal entrance length increased with Reynolds number and Prandtl number, but decreased with Grashof number. This is consistent with the findings of Meyer and Everts [12] and Everts et al. [13] which were obtained using low Prandtl number fluids.

Limited experimental and numerical studies have also been conducted using high Prandtl number fluids, such as glycols and nanofluids. Cheng et al. [24] considered a uniformly heated horizontal rectangular channel and Prandtl numbers ranging from 10 to infinity. They found that higher Rayleigh numbers reduced the required tube length for the onset of mixed convective flow due to enhanced buoyancy-induced secondary flow. Chae and Chung [25] conducted experiments using sulfuric acid-copper sulphate with a Prandtl number of 2094 in short horizontal tubes with length-to-diameter ratios varying between 0.9 and 19.2. They found significant thermal stratification which resulted in different heat transfer characteristics at the top and bottom of the tube. Chou and Hwang [26] numerically investigated mixed convective flow through a horizontal rectangular channel subjected to constant heat flux for Prandtl numbers of 100, 10, 5, 2, 1, and 0.7. Their study revealed distortions in both the velocity and temperature distribution profiles, with the maximum velocity and minimum temperature shifting towards the lower part of the channel due to buoyancy effects. Furthermore, Feng et al. [27] considered silica nanoparticle-ethylene glycol mixtures ($Pr = 20$ to 50) through a horizontal tube subjected to uniform heat flux. They observed that the addition of nanoparticles increased the nanofluid's viscosity, leading to a significant reduction in convective heat transfer.

While extensive research has been conducted on low Prandtl number fluids, extant literature on mixed convective flow of medium and high Prandtl number fluids remains limited. The existing studies focused primarily on highlighting the presence of secondary flow, with some merely noting its effects on the heat transfer coefficient, velocity, and temperature profiles. Furthermore, many of these studies were conducted using short tubes. As noted by Everts et al. [13], short tubes do not capture the full extent of the boundary layer development, even for low Prandtl number fluids such as water. To the authors' best knowledge, no previous studies critically addressed the interplay between buoyancy and viscous effects on the laminar mixed convective thermohydraulic characteristics in long tubes. This is addressed in this study by exploring the thermohydraulic characteristics of varying concentrations of water and propylene glycol mixtures. The analysis focuses specifically on how buoyancy and viscous effects influence the velocity and temperature profiles, vorticity and circulation strength, hydrodynamic and thermal boundary layer development, as well as local Nusselt number and friction factor.

2. Numerical modelling

2.1. Numerical domain and boundary conditions

As illustrated in Fig. 1, a three-dimensional horizontal circular tube was constructed in ANSYS design modeler. It consisted of a solid domain for the copper tube and a fluid domain for the propylene glycol mixtures. The tube was 10 m long with an inner diameter of 5.1 mm and wall thickness of 0.6 mm. The orientation was such that the fluid flowed axially along the z-direction, with the cross-section of the tube being in the x- and y-direction. The fluid was allowed to enter the tube with a uniform axial velocity, V_i, at a uniform temperature, T_i, of 20 °C, while the velocity at the inner wall of the tube was assumed to be zero due to the no-slip condition. The outlet condition of the tube was set as a pressure outlet. The inlet and outlet face of the tube perpendicular to the z-axis were set as adiabatic, and the outer surface of the tube was set as a constant heat flux.

2.2. Governing equations and numerical method

ANSYS Fluent (Release 2022 R2) was used for the numerical simulations, and the flow was assumed to be laminar, single-phase, steady, incompressible, and three-dimensional, without viscous dissipations. Furthermore, gravity as a body force influenced the fluid's overall behaviour and characteristics. The thermophysical properties (density, specific heat capacity, thermal conductivity and viscosity) of the fluid varied with temperature, while the thermal conductivity of the copper tube was assumed to be constant. The conservation equations were thus simplified to:

$$\nabla . \mathbf{u} = 0 \tag{1}$$

$$\rho(\mathbf{u} . \nabla \mathbf{u}) = -\nabla P + \nabla . \left(\mu\left(\nabla \mathbf{u} + (\nabla \mathbf{u})^T\right)\right) + \boldsymbol{F} \tag{2}$$

$$\rho c_p(\mathbf{u} . \nabla T) = \nabla . (k \nabla T) \tag{3}$$

where $\boldsymbol{u}$ is the velocity vector, μ is the dynamic viscosity, ρ is the fluid density, P is the pressure and $\boldsymbol{F}$ is the body force term in the y-direction. The body force vector is expressed as $\boldsymbol{F} = (0, -\rho(T)g, 0)$, due to significant variation in density over a large temperature range (10 °C–100 °C).

The finite volume method (FVM) was used for the spatial discretisation of the governing equations. The coupling between the pressure and velocity fields was handled using the SIMPLE-Consistent algorithm. The momentum and energy equations were temporally discretised using the second-order upwind scheme while the PRESTO scheme was used to numerically discretise the fluid pressure in the fluid domain. To ensure accuracy of the numerical solution in approximating the true behaviour of the flow, convergence was assumed when the residual was below 1×10^{-6}.

2.3. Numerical simulation matrix

To investigate the effect of the Prandtl number, different propylene glycol concentrations were considered, as summarised in Table 1. These mixtures were selected to provide a broad range of thermal and fluid properties. The temperature dependent thermophysical properties of the different mixtures were sourced from the ASHRAE handbook [28] and are summarised in Table 2.

Fig. 2(a) illustrates the Prandtl number ranges of the glycol mixtures for temperature between 20 °C and 100 °C. A general trend is that the Prandtl number decreases with increasing temperature, becoming more pronounced for higher propylene glycol concentrations. This sensitivity of Prandtl number to both temperature and concentration makes it a key parameter in understanding mixed convective heat transfer. As this study focused on single-phase flow, the boiling points of the mixtures had to be accounted for (Fig. 2(b)) because it dictated the maximum heat flux that could be applied.

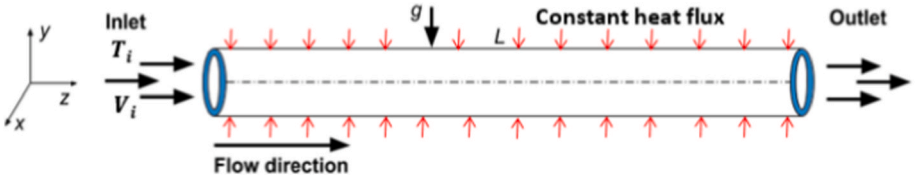

Fig. 1. Schematic of the three-dimensional model indicating the boundary and inlet conditions.

Table 1
Numerical simulation matrix.

Percent Propylene glycol by volume	Heat flux applied to outer surface [W/m^2]	Reynolds number	Inlet temperature [°C]	Prandtl number at inlet
0 % (Pure water)	200 2000	500 500	20	6.8
30 %	200 2000 3500	500 500 250–2000	20	27.4
50 %	200 2000 10 000	500 500 500	20	68.8
70 %	200 1000 2000 3500 10 000	500 250–2000 500 250–2000 250–2000	20	167.2
80 %	200 10 000	500 500	20	257.8
90 %	200 10 000	500 500	20	409.3

2.4. Mesh independence study

A mesh independence study was conducted using water at a heat flux of 1500 W/m^2 and Reynolds number of 1000 by comparing the local laminar Nusselt numbers for different mesh sizes. The initial stage of the discretisation process, with a relatively low number of elements (232 500), began by generating a uniform structured mesh on the tube's cross-section with equal spacing along the tube length, thus resulting in a uniformly coarse mesh. To improve accuracy, general mesh refinement was carried out by controlling the mesh uniformity over the tube's cross-section (Fig. 3(a)), and controlling its distribution along the tube length (Fig. 3(b)). A bias factor of 1.5 was used along the tube length to increase mesh density in the entrance region to accurately capture the boundary layer development.

Using this bias factor, the node spacing was adjusted such that the total number of elements roughly doubled with each refinement and the resulting Nusselt numbers for the various mesh sizes are presented in Fig. 4. For the first three mesh refinements (232 500, 577 500 and 1 170 000) there was a marked difference, while the Nusselt numbers of the remaining three mesh sizes were all very close to each other. As the difference between the mesh of 3 780 000 elements and the next finer

Table 2
Thermophysical properties of propylene glycol concentrations by volume for 10 °C–100 °C.

Thermophysical Properties	Concentrations in Volume Percent Propylene Glycol					
	0%	30%	50%	70%	80%	90%
ρ [kg/m^3]	998.2–952.6	1029.5–977.5	1044.1–984.1	1053.6–987.1	1054.4–989.1	1052.3–987.0
k [W/m.K]	0.6017–0.6790	0.4316–0.4780	0.3416–0.3700	0.2662–0.2810	0.2371–0.2460	0.2143–0.2180
C_p [J/(kg.K)]	4147–4267	3848–4068	3532–3841	3117–3515	2876–3319	2600–3089
μ [kg/m.s]	0.001002–0.000280	0.003076–0.000530	0.006664–0.000790	0.014276–0.001180	0.021251–0.001420	0.033729–0.002000

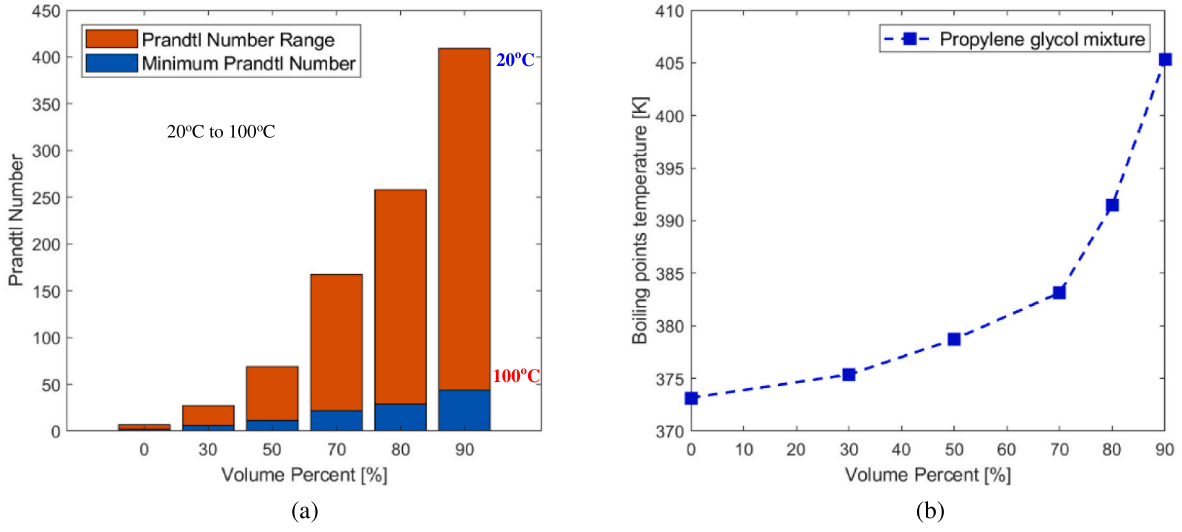

Fig. 2. (a) Prandtl numbers ranges between 20 °C and 100 °C and (b) boiling temperatures at atmospheric pressure for various propylene glycol concentrations.

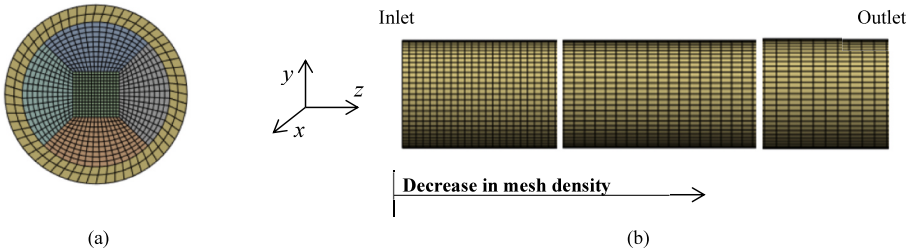

Fig. 3. Example of (a) cross-sectional mesh and (b) non-uniform mesh distribution along tube length.

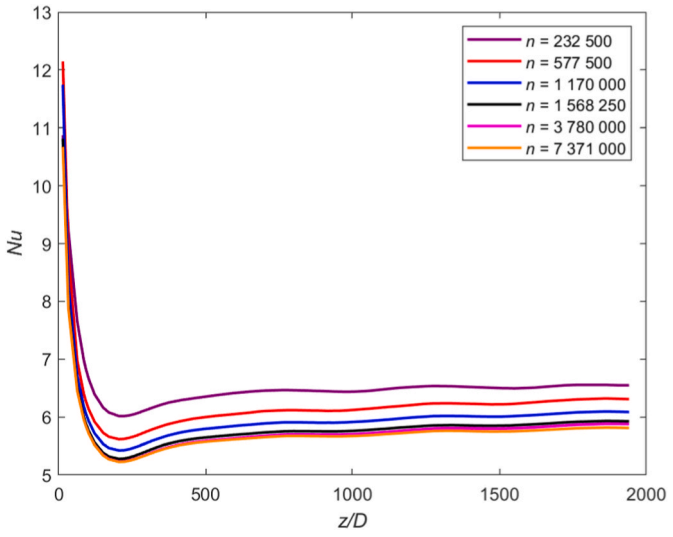

Fig. 4. Comparison of the local laminar mixed convective Nusselt number as a function of axial position for different mesh sizes at a heat flux of 1500 W/m^2 and Reynolds number of 1000.

mesh of 7 371 000 was only 2 %, the mesh with 3 780 000 elements was selected in the interests of computational efficiency while providing sufficient numerical accuracy.

3. Data reduction

The local wall temperature, T_w, along the tube length was obtained by taking an arithmetic average of the local temperature around the circumference of the tube:

$$T_w = \frac{1}{\pi D}\int_0^{\pi D} T(p)\, dp \tag{4}$$

where p is the perimeter of the tube cross-section and D is the inner diameter of the tube.

The local mean fluid temperature, T_m, was calculated using the mass-weighted average across cross-sectional planes along the tube length:

$$T_m = \frac{\int_A \rho w T dA}{\int_A \rho w dA} \tag{5}$$

where A is the cross-sectional area of the tube, ρ is the fluid density and w is the velocity in z-direction.

The local heat transfer coefficient, h, was calculated using the local mean fluid temperature and the local wall temperature.

$$h = \frac{\dot{q}}{T_w - T_m} \tag{6}$$

where $\dot{q}$ is the heat flux on the inside of the tube.

The local Nusselt number, Nu, was computed from the local heat transfer coefficient:

$$Nu = \frac{hD}{k} \tag{7}$$

where D is the inner diameter of the tube and k is the thermal conductivity of the fluid obtained at the mean fluid temperature.

To characterise the flow regime along the tube length and describe the relationship between the thermal diffusivity and momentum diffusivity, the Reynolds number (Re) and the Prandtl number (Pr) were determined as follows:

$$Re = \frac{\dot{m}D}{\mu A_c} \tag{8}$$

$$Pr = \frac{\mu C_p}{k} \tag{9}$$

where $\dot{m}$ is the fluid's mass flow rate, μ is the dynamic viscosity at the mean fluid temperature, A_c is the cross-sectional area of the tube, and C_p is the specific heat capacity at the mean fluid temperatures.

The heat transfer results were also examined in terms of the Colburn j-factor as:

$$j = \frac{Nu}{Re\, Pr^{\frac{1}{3}}} \tag{10}$$

The local buoyancy force, BF, was computed as:

$$BF = \rho g \beta (T_w - T_m) \tag{11}$$

where g is gravitational acceleration, β is the thermal expansion coefficient and ρ is the fluid density evaluated at local mean fluid temperature.

The Grashof number, Gr, representing buoyancy effects was determined as:

$$Gr = \frac{g\beta(T_w - T_m)D^3}{\nu^2} \tag{12}$$

where ν is the kinematic viscosity of the fluid.

The secondary flow strength along the tube length was computed as the ratio of cross-sectional secondary flow velocity to the total velocity:

$$\Psi = \frac{\sqrt{u^2 + v^2}}{\sqrt{u^2 + v^2 + w^2}} \tag{13}$$

where u, v, and w are the velocity in x-, y-, and z-directions.

The vorticity magnitude at a cross-section along the tube length was calculated as the square root of the sum of the squares of the vorticity components at that cross-section:

$$|\omega| = \sqrt{\omega_x^2 + \omega_y^2 + \omega_z^2} \tag{14}$$

where ω_x and ω_y are the radial and circumferential vorticity component and ω_z is the axial vorticity component.

The circulation strength, Γ, was calculated locally as the integral of the vorticity magnitude over the local cross-sectional area along the tube length:

$$\Gamma = \int_A |\omega| dA \tag{15}$$

The local friction factor was determined as:

$$f = \frac{2\Delta P D}{z \rho V^2} \tag{16}$$

where, ΔP is the local pressure drop, z is axial position along the tube, V is the local fluid velocity along the tube length, and ρ is local fluid density along the tube length.

4. Validation

To validate the local Nusselt numbers, the forced convection results for water at a heat flux of 1000 W/m^2 and a Reynolds number of 1800 were compared with the theoretical fully developed Nusselt number of 4.36, the correlation of Shah and London [1], and the experimental results of Meyer and Everts [12]. The results in Fig. 5 show a good agreement with both the correlation and experimental data, with an average deviation of less than 5% and 3%, respectively. The average fully developed Nusselt number between $z/D = 600$ and $z/D = 1120$ was 4.38 which was within 0.34% of the theoretical Nusselt number of 4.36.

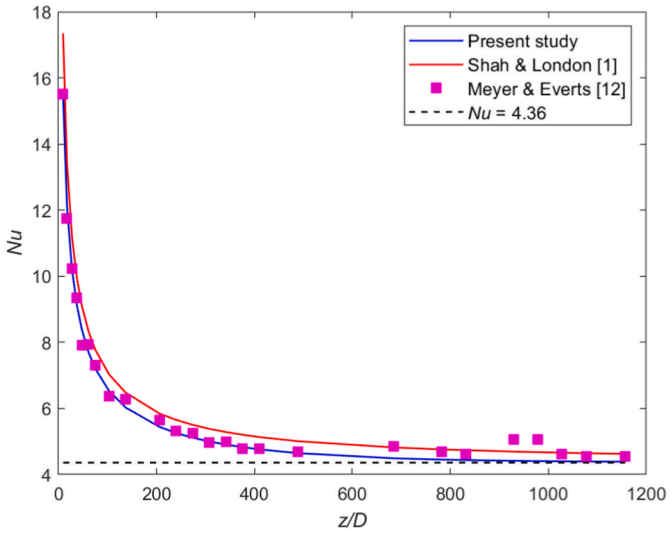

Fig. 5. Comparison between the local forced convective Nusselt numbers for water at a heat flux of 1000 W/m^2 and Reynolds number of 1800 with the correlation of Shah and London [1], experimental data of Meyer and Everts [12], and the theoretical fully developed value of 4.36.

Furthermore, the mixed convection results for water at a heat flux of 6000 W/m^2 and a Reynolds number of 1600 were compared to the experimental data of Meyer et al. [11] as well as the correlation of Meyer and Everts [12]. Fig. 6 shows that the results correlated well with both the experimental data and the correlation with an average deviation of less than 3% and 2%, respectively. As the numerical model was able to accurately simulate the heat transfer characteristics of both forced and mixed convective flow using water, reliable results were also expected for water-propylene glycol mixtures.

5. Results

5.1. Forced convective heat transfer characteristics

To achieve forced convective flow at a Reynolds number of 500, a constant heat flux of 200 W/m^2 was applied. The results were plotted on the flow regime map of Everts and Meyer [29] in Fig. 7, which confirmed that the heat transfer of the propylene glycol mixtures was governed by forced convective flow.

Fig. 8 compares the cross-sectional temperature distributions for different propylene glycol mixtures at axial positions of $z/D = 400$ and $z/D = 1900$ (developing flow and fully developed flow, respectively, based on Fig. 5). As the tube was heated at a constant heat flux, Fig. 8(a) indicates that the temperature of the fluid near the wall was higher than near the centreline. When increasing the propylene glycol concentration, heat transfer became concentrated near the wall and a larger core region remained unaffected by temperature increases. The magnitude of the wall and fluid temperatures also decreased with increasing glycol concentration. As the flow developed along the tube length, Fig. 8(b) indicates that the temperature distribution from the wall to the centre of the tube became more uniform. However, for 90% propylene glycol there was still a portion of the core flow that remained unaffected by heat transfer from the tube wall.

Fig. 8(c) and (d) compare the cross-sectional temperature gradient for different propylene glycol concentrations. The vertical black arrow in Fig. 8(c) indicates a gradient of zero, meaning that the core of the 50% and 90% propylene glycol mixtures remained isothermal at the initial bulk temperature. This resulted in a steep temperature gradient near the wall, as indicated by the magenta and orange arrows. This was attributed to the combined effects of lower thermal conductivity and higher viscosity of propylene glycol, confining the thermal boundary layer close to the wall. Conversely, the 0% and 30% mixtures exhibited a gradual temperature variation at the core, as shown by the red and blue arrows, respectively.

As the fluid flowed along the tube length, the thermal boundary layer thickness increased due to continuous heat transfer from the wall. The isothermal core region decreased, and a larger portion of the cross-sectional flow became involved in the heat transfer process, which is evident from the temperature gradient plots in Fig. 8(c) and (d). The core temperatures in Fig. 8(b) were generally higher than in Fig. 8(a) due to heat absorption along the tube length, however, as indicated by the black arrow in Fig. 8(d), an isothermal region existed for the 90% mixture due to its low thermal conductivity. On the other hand, water's higher thermal conductivity facilitated heat transfer and thermal boundary layer development which resulted in a uniform cross-sectional temperature distribution for 0% propylene glycol (pure water).

To gain a deeper understanding on the influence of fluid properties,

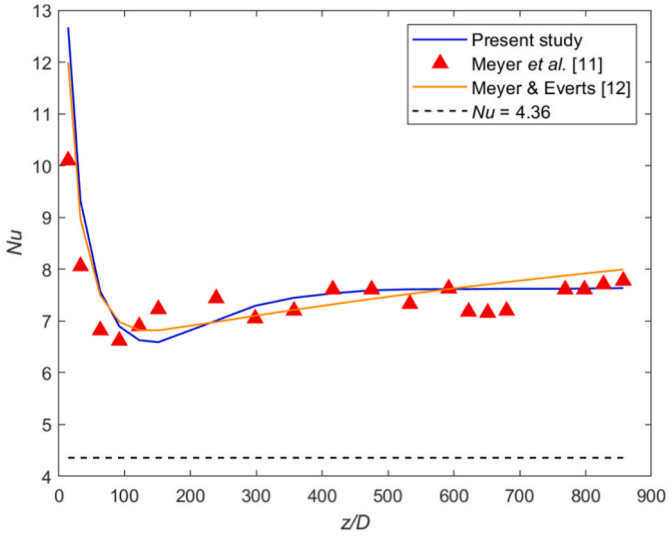

Fig. 6. Comparison of the local mixed convective Nusselt numbers for water at a heat flux of 6000 W/m^2 and Reynolds number of 1600 with the experimental data of Meyer et al. [11], correlation of Meyer and Everts [12], and the theoretical fully developed value of 4.36.

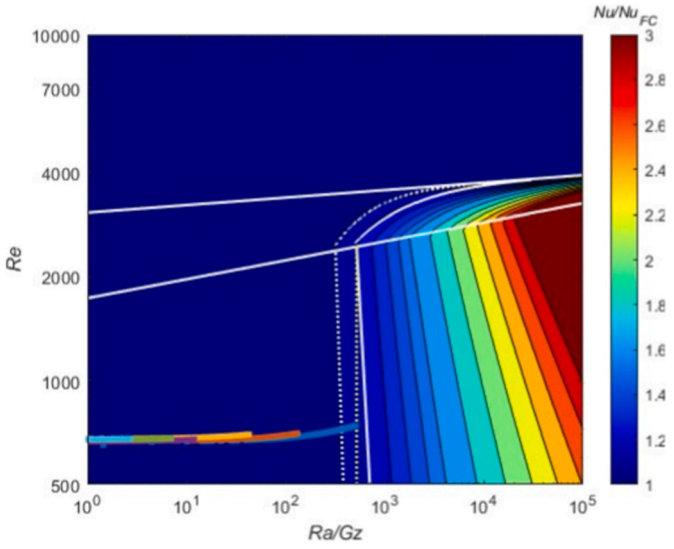

Fig. 7. Prediction of forced convective flow for different propylene glycol concentrations at a heat flux of 200 W/m^2 and a Reynolds number of 500 using the flow regime map of Everts and Meyer [29].

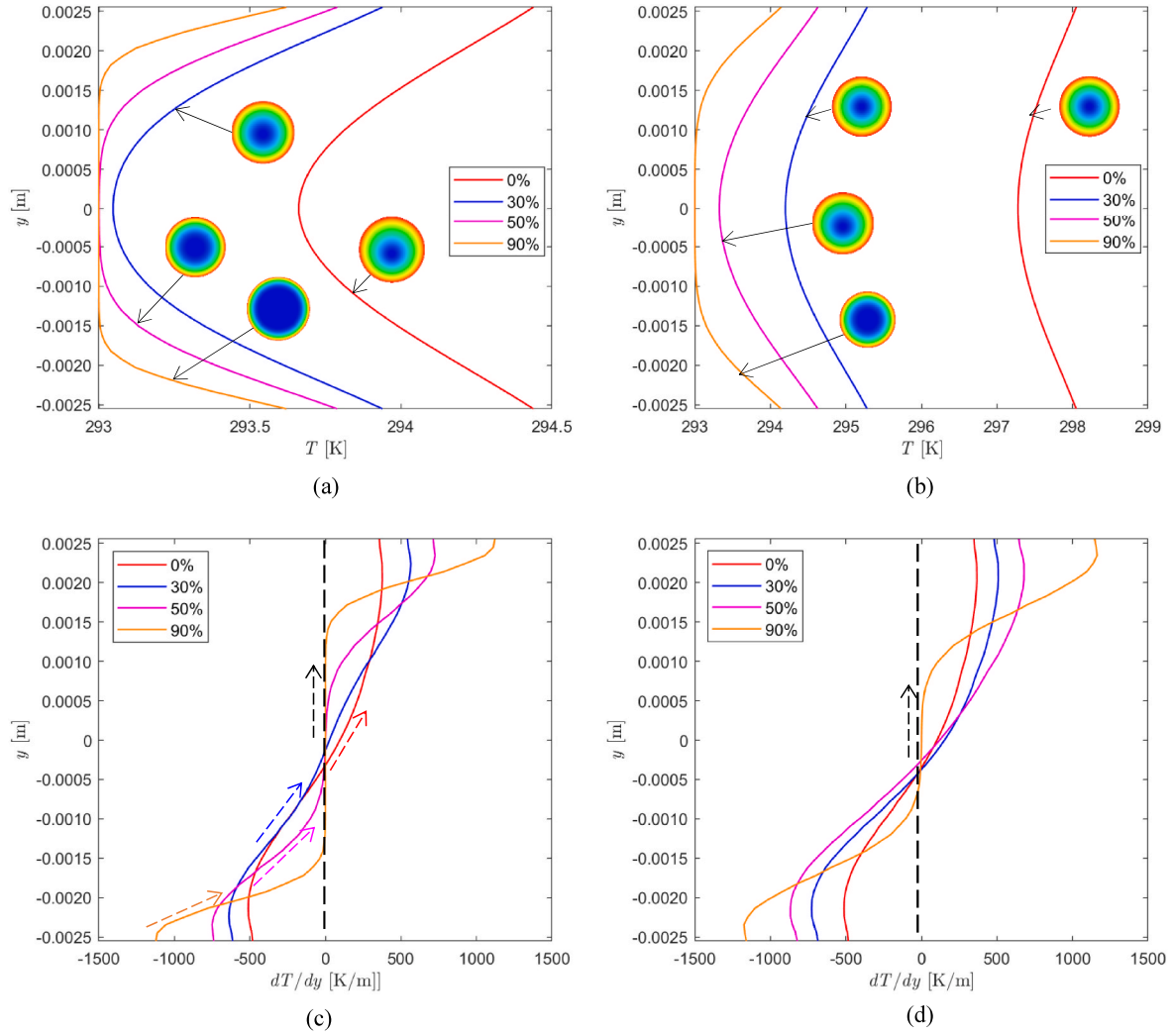

Fig. 8. Laminar forced convective cross-sectional temperature distributions at (a) $z/D = 400$ and (b) $z/D = 1\,900$, as well as the corresponding temperature gradients at (c) $z/D = 400$ and (d) $z/D = 1\,900$, for different propylene glycol mixtures at a heat flux of 200 W/m^2 and a Reynolds number of 500.

Fig. 9 compares the viscosity and thermal conductivity variation along the tube length for different propylene glycol mixtures. The blue and red circular markers on the viscosity contour profile represent the tube centre and near-wall region (taken as 90% of the tube radius), respectively, from which the viscosity distributions (blue and red lines) were obtained.

A general trend in this figure is that increased propylene glycol concentrations led to increased viscosities, decreased thermal conductivities, and larger cross-sectional variations in the fluid properties. As the tube was heated at a constant heat flux, the fluid in the near-wall region had a higher temperature than that at the centre. This resulted in a decrease in viscosity and increase in thermal conductivity, as indicated in Fig. 9(a). This in turn also affected the development of the thermal boundary layer, which will be discussed in more detail in Section 5.3. Near the inlet, where the flow was still developing, the increase in wall temperature was greater than the increase in bulk fluid temperature, which resulted in a gradual increase in the cross-sectional wall-fluid thermal conductivity difference. As the propylene glycol concentration increased to 50% (Fig. 9(c)) and 90% (Fig. 9(d)), the variation in the cross-sectional thermal conductivity along the tube length became more significant. Furthermore, when comparing Fig. 9(a) and (d), it can be seen that for 0% glycol (pure water), the thermal conductivity was approximately three times higher, which assisted with heat transfer from the wall to centre of the tube and explains the smaller and uniform cross-sectional thermal conductivity differences along the tube length.

Fig. 9 also indicates that the wall-fluid viscosity difference along the tube length increased for increased propylene glycol concentration. This can be attributed to reduced thermal diffusion from the wall, caused by a decrease in the thermal conductivity of the fluids as the glycol concentration increased, leading to greater wall-fluid temperature difference. For the 90% glycol mixture, Fig. 9(d) indicates that, due to the low thermal diffusivity, heat transfer toward the tube centre was minimal which resulted in the viscosity at the centreline to be nearly constant along the tube length and approximately two orders of magnitude higher than for water (Fig. 9(a)). Therefore, despite the significant cross-sectional temperature differences, the flow was still dominated by forced convection (as indicated on the flow regime map in Fig. 7), due to the high viscosity which dampened any buoyancy effects arising from cross-sectional temperature and density differences.

5.2. Mixed convective heat transfer characteristics

While the forced convective analysis provided an understanding of the heat transfer characteristics in propylene glycol mixtures, it becomes crucial to investigate mixed convective behaviour when higher heat fluxes are applied. This involves buoyancy effects that significantly alter the heat transfer characteristics and flow behaviour [29]. In this section,

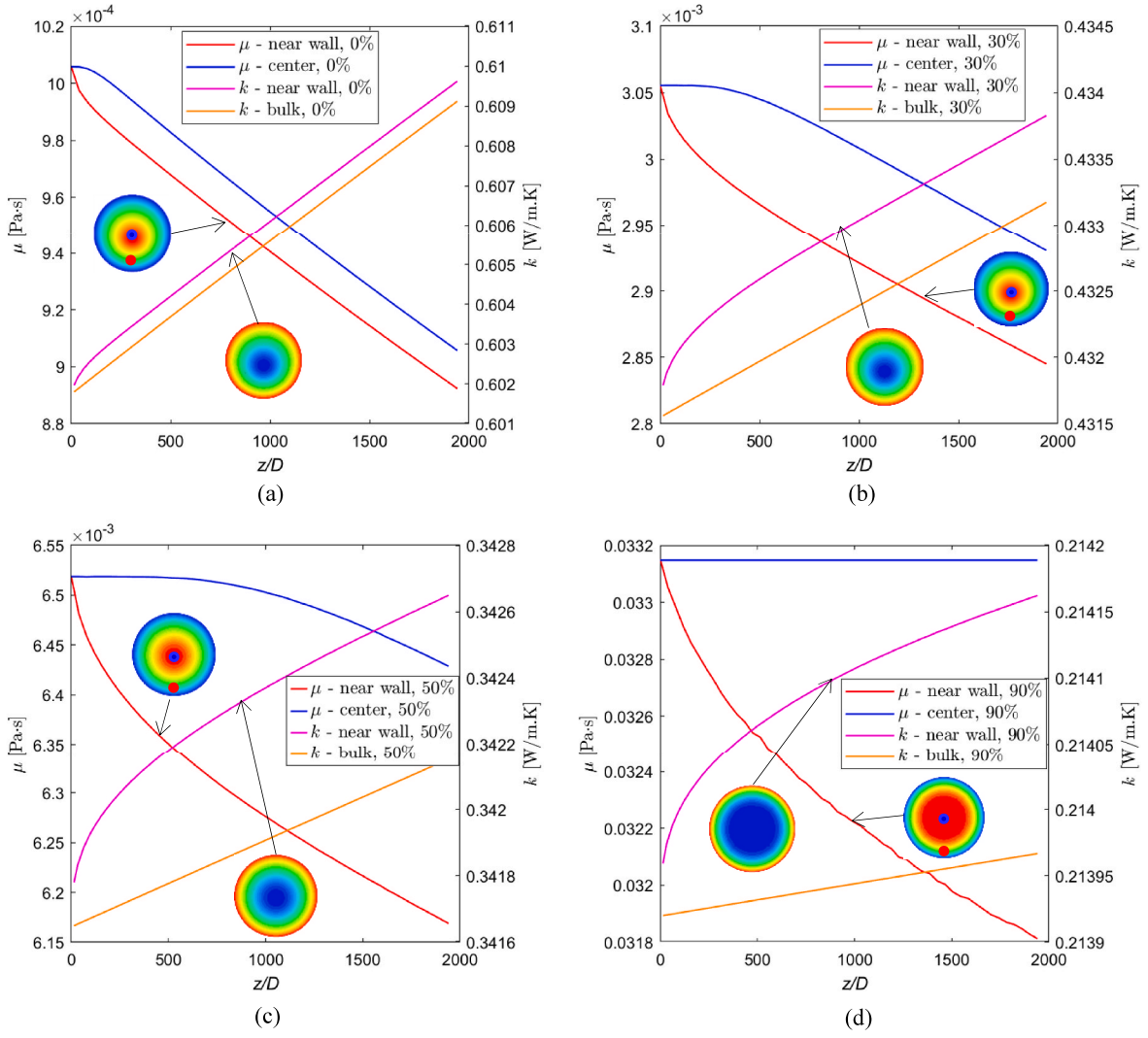

Fig. 9. Comparison of the axial viscosity and thermal conductivity profiles at a heat flux of 200 W/m^2 and Reynolds number of 500 for (a) 0%, (b) 30%, (c) 50%, and (d) 90% propylene glycol mixtures.

the cross-sectional temperature, density, local buoyancy forces, and secondary flow strength indicators are analysed to comprehensively investigate the mixed convective behaviour of high Prandtl number fluids.

To visualise the mixed convective behaviour and corresponding effects on the cross-sectional temperature, density, and flow fields, the symmetry introduced by uniform heating was utilised. Fig. 10 uses a symmetric cross-sectional split with temperature contours on the left, density contours on the right, together with superimposed secondary flow streamlines. These are depicted at various positions along the tube length for different propylene glycol concentrations.

Near the tube inlet (z/D = 20), the temperature variation was confined near the wall, indicating a thin thermal boundary layer which further decreased in thickness with increasing glycol concentration. This also resulted in the density gradient being confined within the thermal boundary layer. As the propylene glycol concentration increased, Fig. 9 showed that the rate of heat transfer from the wall decreased due to the increase in the fluid's thermal resistance. Due to the relatively small cross-sectional temperature differences near the tube inlet, the streamlines indicate minimal to no secondary flow patterns as forced convection dominated for all propylene glycol concentrations.

As the fluid flowed downstream (z/D = 120, 400, 1000, and 1900), the fluid temperatures increased causing the temperature contours to extend inward toward the core region, signifying an increase in thermal boundary layer thickness. The increasing wall-fluid temperature difference also resulted in increased cross-sectional density variations that led to buoyancy-induced secondary flow. As the tube wall was heated, the fluid near the wall had a higher temperature and lower density, causing the fluid to move upwards along the tube wall, while the cooler, denser fluid near the tube centre moved downwards. This led to the formation of two counter-rotating vortices that enhanced mixing and heat transfer [30]. Furthermore, as the fluid flowed along the tube length, the accumulation of the warmer fluid near the top shifted the vortical activity downwards, leading to steep temperature and density gradients near the bottom and asymmetric (top and bottom) temperature and density profiles.

It follows from Fig. 10 that as the propylene glycol concentration increased, the wall-fluid temperature difference increased, resulting in a steeper temperature gradient and the expectation of increased buoyancy effects. However, as indicated by the streamlines at z/D = 1 900, buoyancy effects were most pronounced in the 0% propylene glycol mixture and diminished with increasing propylene glycol concentration due to the increased viscosity that suppressed buoyancy-induced secondary flow. Therefore, to further investigate the effect of Prandtl number on the cross-sectional mixed convective behaviour, Fig. 11 compares the cross-sectional temperature profiles at z/D = 400 (Fig. 11

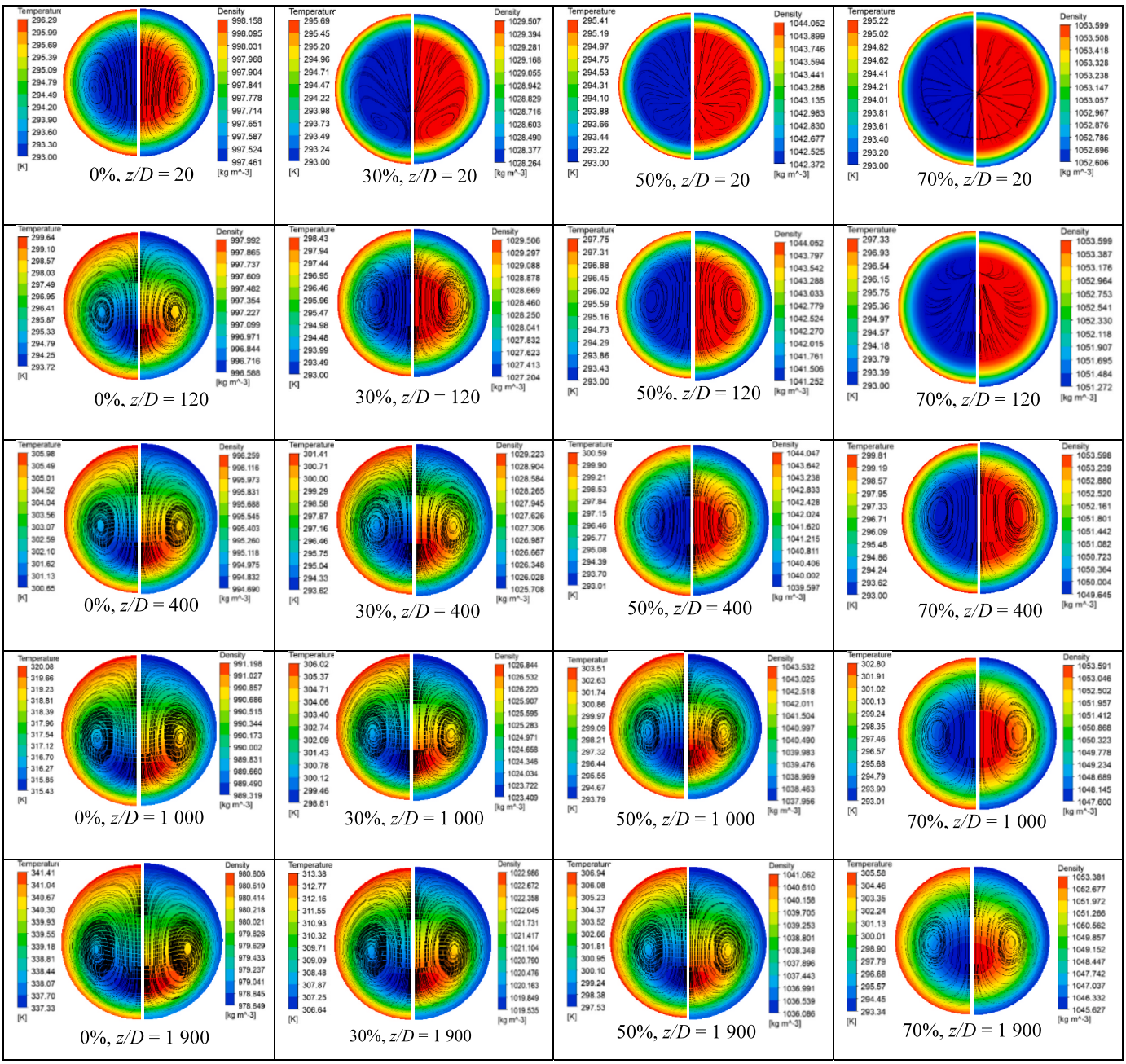

Fig. 10. Cross-sectional temperature (left half) and density (right half) contours together with secondary flow streamlines at different axial positions for different propylene glycol concentrations at a heat flux of 2000 W/m^2 and Reynolds number of 500.

(a)) and $z/D = 1900$ (Fig. 11(b)), for developing and fully developed flow, respectively. A general trend is that as the propylene glycol concentration decreased, the position of the minimum core temperature (points A-H) shifted downwards. As shown in Fig. 10, this asymmetric profile led to a steep temperature gradient in the lower half of the tube, indicating efficient heat transfer due to the vortical activity, and a significantly smaller gradient in the upper half. Point A in Fig. 11(a) indicates that for a 70% propylene glycol concentration, the minimum core temperature was located at the centre, which corresponds to general forced convective trends. However, as the propylene glycol concentration decreased (points B-D) and the flow developed along the tube length (point E in Fig. 11(b)), buoyancy effects became significant and the position of the minimum core temperature shifted downwards. This trend was most noticeable for 0% propylene glycol, due to the higher thermal conductivity and lower viscosity of water which facilitated the development of buoyancy effects.

Fig. 12 compares the local buoyancy force (calculated using Equation (11)) in forced (Fig. 12(a)) and mixed (Fig. 12(b)) convective flows for different propylene glycol mixtures along the tube length. A general trend is that the buoyancy force became significantly stronger as the propylene glycol concentration increased. At 70%, 80%, and 90% propylene glycol concentration, the buoyancy force was on average 74.5%, 78.4% and 79.8% higher for forced convective flow, and 67.2%, 72.4% and 73.5% higher for mixed convective flow, compared to the 0% propylene glycol concentration. In Fig. 12(a), the buoyancy force was weak near the tube inlet and gradually increased along the tube length due to the increased wall-fluid temperature difference. Furthermore, the magnitude of the buoyancy force was approximately an order of magnitude less than for the mixed convective results in Fig. 12(b), which corresponded well with the order of magnitude in difference in heat

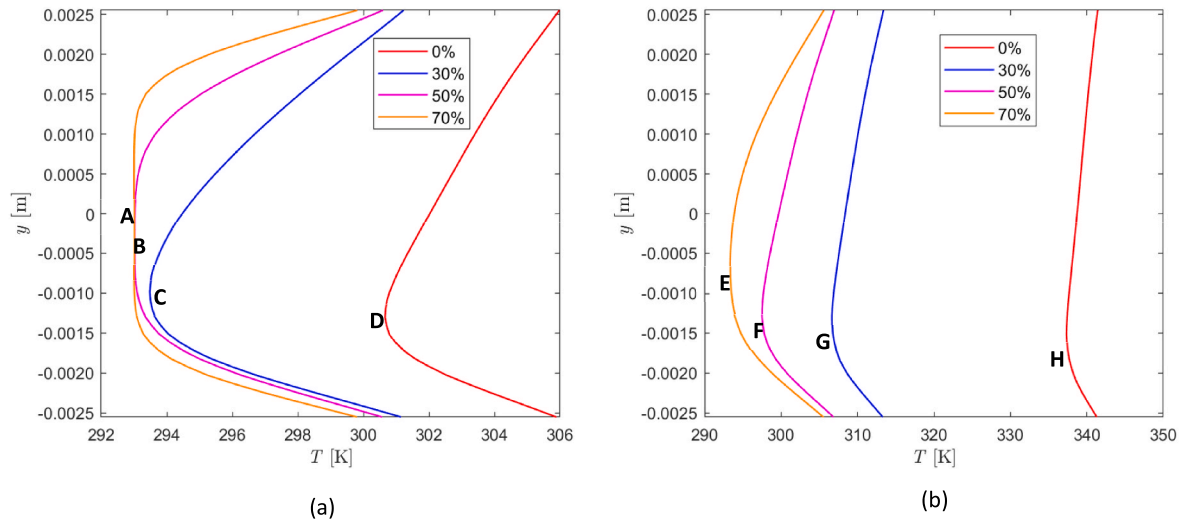

Fig. 11. Laminar mixed convective cross-sectional temperature distribution for different propylene glycol concentrations at a heat flux of 2000 W/m^2 and Reynolds number of 500 at (a) $z/D = 400$, and (b) $z/D = 1900$.

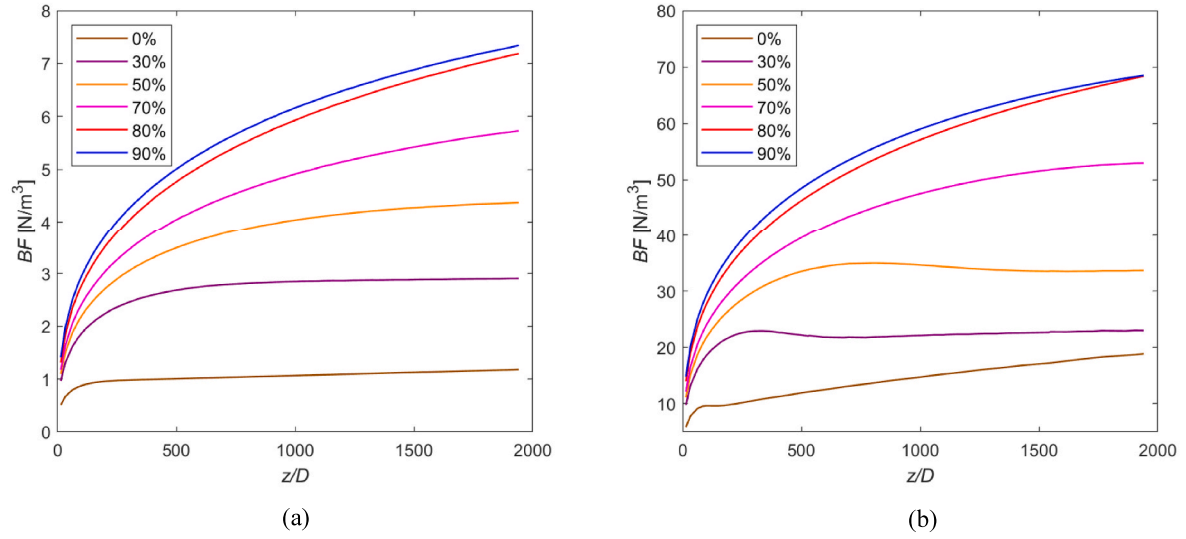

Fig. 12. Comparison of the buoyancy force as a function of the axial position for different propylene glycol concentrations at a Reynolds number of 500 and heat flux of (a) 200 W/m^2 (forced convection) and (b) 2000 W/m^2 (mixed convection).

fluxes that were used.

Fig. 12(b) indicates that for 0%, 30%, and 50% propylene glycol mixtures, the buoyancy force increased rapidly near the tube inlet, reached a peak and then decreased slightly before stabilising at an approximately constant gradient which decreased with increasing glycol concentration. Due to the higher thermal conductivity and lower viscosity of these propylene glycol mixtures, significant buoyancy effects developed earlier along the tube length, which explains why the peak occurred earlier with decreasing propylene glycol concentration. Once buoyancy effects became significant, radial fluid mixing was enhanced, which in turn decreased the cross-sectional temperature gradient (which is proportional to the buoyancy force), leading to a slight decrease in buoyancy force. However, as the fluid continued to flow along the heated tube length, the fluid temperature increased which led to continued increase in thermal conductivity and decrease in density and viscosity. This increased buoyancy-induced secondary flow and explains why the buoyancy force increased again. Given the fact that an increase in propylene glycol concentration led to decreased buoyancy-induced secondary flow (as shown in Fig. 10) due to increased fluid viscosity, the increasing buoyancy force with increasing propylene glycol concentration for both forced and mixed convective flows was initially unexpected. However, this was due to changes in heat dissipation driven by the fluid's thermal conductivity. As shown in Fig. 9, an increase in propylene glycol concentration led to decreased thermal conductivities and thus larger cross-sectional temperature and density variations (Fig. 10), which resulted in an artificial increase in buoyancy force not necessarily representative of the actual buoyancy effects.

To gain a deeper understanding of how the interplay between buoyancy and fluid viscosity affects the flow field and heat transfer, Fig. 13 compares the secondary flow strength (Equation (13)) and circulation strength (Equation (15)) along the tube length, as well as the vorticity magnitude (Equation (14)) at $z/D = 1900$ for different propylene glycol concentrations. For concentrations of 0%, 30%, and 50%, the secondary flow strength (black lines) revealed three distinct regions: (1) gradual increase from the tube inlet to a peak (developing region), (2) decrease to a minimum (suppression region), followed by (3) an increase toward the tube outlet (enhancement region). In contrast, for higher propylene glycol concentrations (70%, 80%, and 90%), the

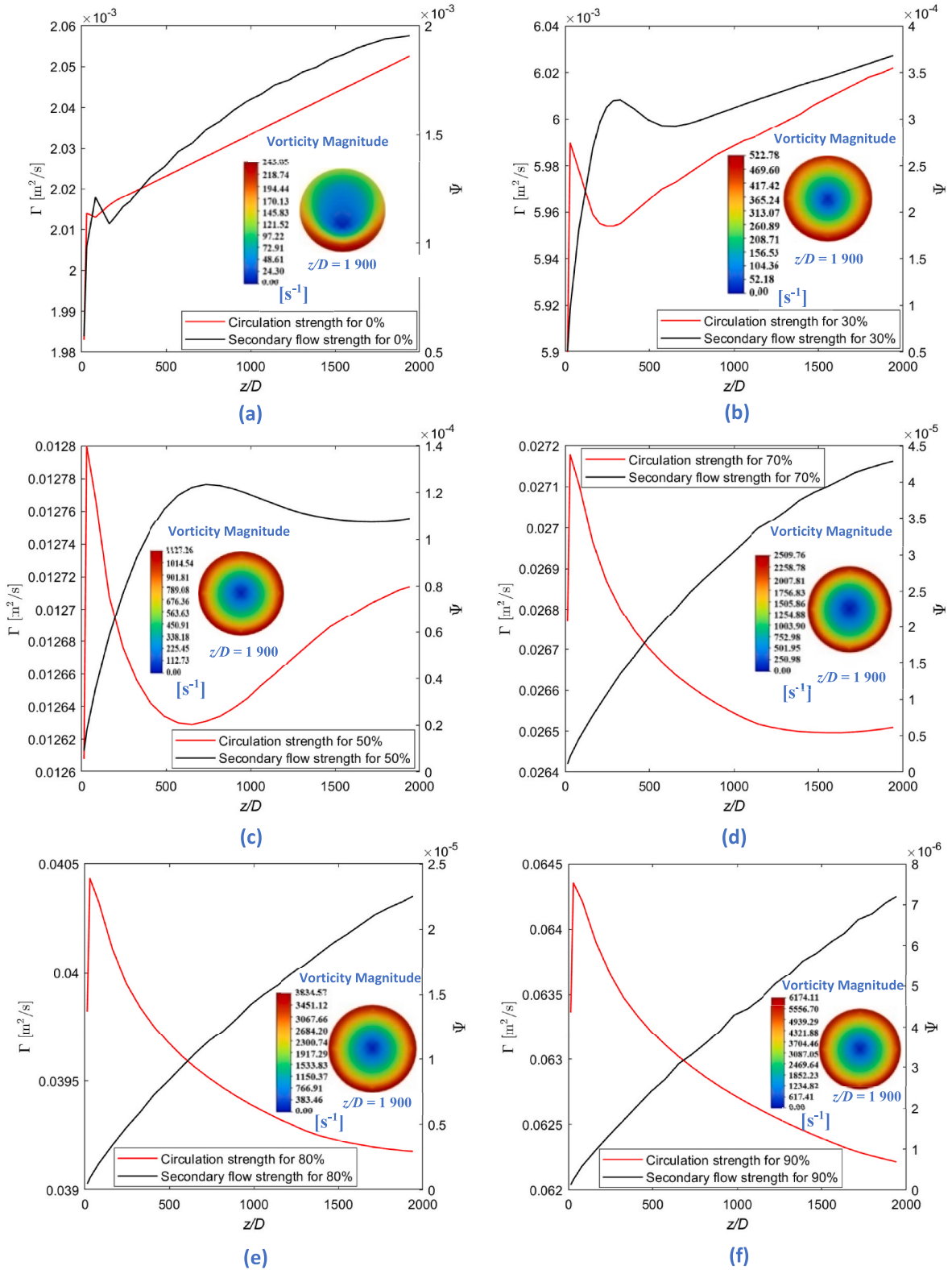

Fig. 13. Comparison of secondary flow strength (black lines), circulation strength (red lines), and vorticity magnitude (contour plots) at a heat flux of 2000 W/m^2 and Reynolds number of 500 for (a) 0%, (b) 30%, (c) 50%, (d) 70%, (e) 80% and (f) 90% propylene glycol mixtures.

secondary flow strength increases monotonically toward the tube outlet, indicating an elongated developing region. This trend can be attributed to the interplay between buoyancy forces and fluid viscosity along the tube length.

Near the tube inlet, the secondary flow strength and buoyancy force were minimal due to the very small temperature differences, as seen in Fig. 12. As the fluid progressed downstream, its overall temperature increased, due to heat transfer from the tube wall, leading to a significant buoyancy force that overcame fluid viscosity, resulting in an increase in secondary flow strength along the tube length. For low

propylene glycol concentrations (0%, 30%, and 50%), where the fluid viscosity is relatively low, this resulted in a peak towards the tube inlet. However, the increased mixing resulting from this secondary flow temporarily decreased the wall-fluid cross-sectional temperature differences and resulted in temporary suppression of the secondary flow strength. Notably, the absolute value of the gradient of this suppression region decreased as the propylene glycol concentration increased due to increase in the fluid viscosity, resulting in a larger region of suppression. As the fluid was heated along the tube length, the buoyancy force increased, due to an increased wall-fluid temperature difference, further strengthening and enhancing the secondary flow. The gradient of this enhancement region was again affected by the propylene glycol concentration, decreasing as the viscosity increased.

In higher propylene glycol concentrations (70%, 80%, and 90%), where the temperature gradient remained steep along the tube length due to the fluid's higher viscosity and lower thermal conductivity, the required tube length for buoyancy-induced secondary flow increased. These higher propylene glycol concentrations experienced weaker secondary flow strengths (reductions of up to 95%) as secondary flow development was suppressed by the increased viscosity. For these fluids, the tube was not sufficiently long to reach the peak secondary flow strength.

As shown in Fig. 11, a high temperature gradient which enhanced density variations occurred near the tube wall and resulted in a significant buoyancy force and high vorticity. For 0% propylene glycol, the vorticity contour plot in Fig. 13(a) indicates lower vorticity at the upper part of the tube. This can be attributed to the strong secondary flow which caused the vortices to move downwards (as shown in Fig. 10) and the lower part of the tube to be more active. However, as the propylene glycol concentration increased, the vorticity became symmetrically confined near the wall due to increased fluid viscosity which suppressed the secondary flow.

The circulation strength (red lines), quantifies the net rotational effect. At the tube inlet, initial vorticity existed due to the no-slip condition at the wall which resulted in an increase in circulation strength. However, this initial vorticity was quickly dissipated which caused the

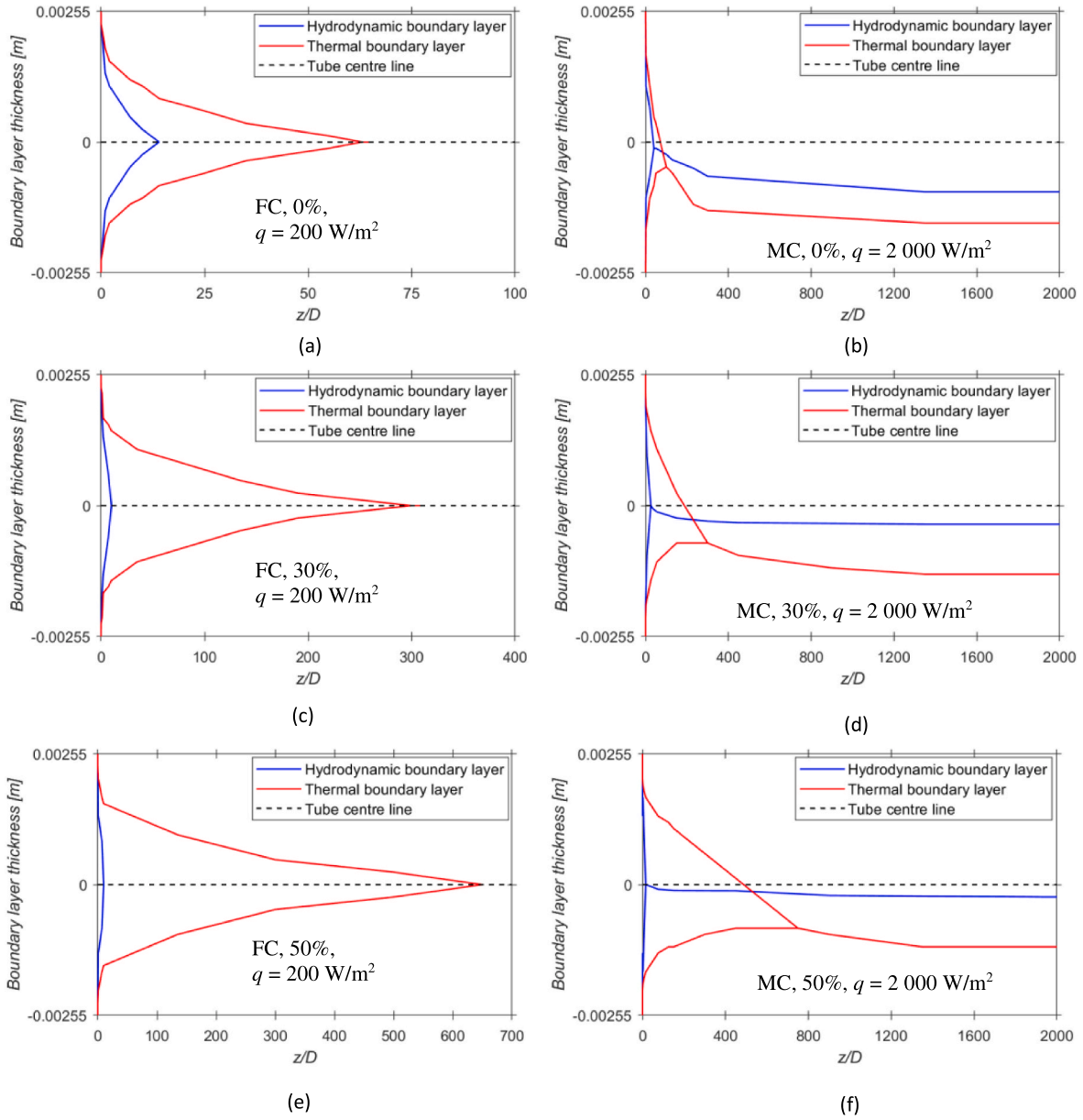

Fig. 14. Hydrodynamic and thermal boundary layers at a Reynolds number of 500 with heat fluxes of 200 W/m^2 (forced convection (FC), left column) and 2000 W/m^2 (mixed convection (MC), right column) for propylene glycol concentrations of (a) 0% FC, (b) 0% MC, (c) 30% FC, (d) 30% MC, (e) 50% FC, and (f) 50% MC.

circulation strength to decrease. As the fluid was heated along the tube length, buoyancy-induced vorticity was produced near the wall and redistributed through secondary flow across the cross-section, leading to an increase in circulation strength as the flow developed. For high propylene glycol concentrations (70%, 80%, and 90%), buoyancy effects and the corresponding thermal boundary layer developed slower along the tube length (as will be shown in Fig. 14) due to the lower thermal conductivity of propylene glycol compared to water. Therefore, for the given tube length, sufficient buoyancy-induced vorticity near the wall could not develop to increase the circulation strength along the tube length.

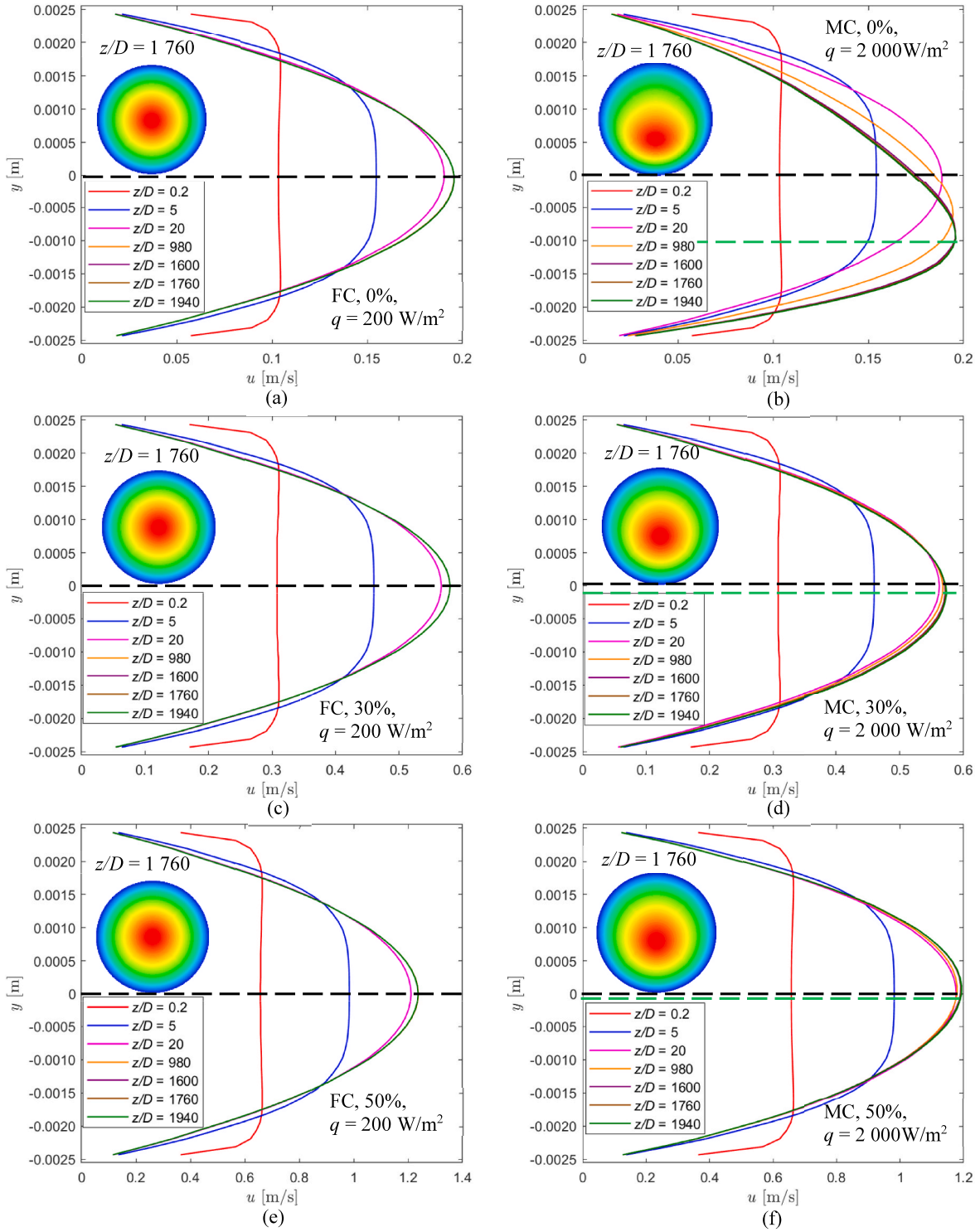

Fig. 15. Cross-sectional velocity profile along the tube length at Reynolds number of 500 with heat fluxes of 200 W/m^2 (forced convection (FC), left column) and 2000 W/m^2 (mixed convection (MC), right column) for propylene glycol concentrations of (a) 0% FC, (b) 0% MC, (c) 30% FC, (d) 30% MC, (e) 50% FC, and (f) 50% MC.

5.3. Hydrodynamic and thermal boundary layer development

The method of Everts et al. [13] was used to investigate the hydrodynamic and thermal boundary layers. A vertical plane across the tube centre was used as a reference. The core region was dominated by parallel flow from the inlet (before the hydrodynamic boundary layer merged) and unaffected by heat transfer from the tube wall (before the thermal boundary layer merged). Therefore, the velocity and temperature gradients in the *y*-direction were approximately zero and only changed at the edge of the respective boundary layer, respectively. The merging point of the respective boundary layers corresponded to the minimum value of the velocity and temperature gradients.

Fig. 14 compares the hydrodynamic (blue) and thermal (red) boundary layers at a Reynolds number of 500 for forced and mixed convective flow. The thermal boundary layer thickness increased from the tube inlet and merged at the tube centre line for forced convective flow (Fig. 14(a)–(c), and (e)), while Fig. 14(b)–(d), and (f) indicate that the mixed convective thermal boundary layer merged below the centre line. This merging point continued downwards along the tube length before becoming constant. For both forced and mixed convective flow, the axial position at which the thermal boundary layer merged increased with increasing propylene glycol concentration. This can be attributed to decreased thermal conductivity (Fig. 9) which resulted in slower thermal diffusion from the wall and consequently slower boundary layer development. Furthermore, with increasing propylene glycol concentration, the increased viscosity dampened buoyancy effects (Figs. 10 and 13), despite stronger buoyancy forces (Fig. 12). Hence, the merging position moved upward towards the centre line.

Similar to the thermal boundary layers, the forced convective hydrodynamic boundary layers merged at the tube centre line, while there was a slight downward shift for mixed convective flow. The mixed convective merging position also continued to move downwards before becoming constant along the tube length, but the downward shift was less pronounced than for the thermal boundary layer. An interesting observation in Fig. 14 was that, unlike for the thermal boundary layer, both the forced convective and mixed convective hydrodynamic boundary layers merged earlier along the tube length for increased propylene glycol concentration and the axial position at which the merging position became constant occurred earlier too. The hydrodynamic boundary layer represents the relative influence of inertia and viscosity in the fluid flow. As a higher viscosity reduces the effect of inertia, it enhances momentum diffusion within the fluid which leads to faster growth of the hydrodynamic boundary layer. This explains why the hydrodynamic boundary layer merged earlier along the tube length, indicating a decreased hydrodynamic entrance length for increasing propylene glycol concentrations.

To further investigate the effect of high Prandtl numbers on the hydrodynamic boundary development, Fig. 15 compares the cross-sectional velocity profiles of different propylene glycol mixtures for forced convective (Fig. 15(a)–(c) and (e)) and mixed convective (Fig. 15 (b)–(d) and (f)) flows. A general trend from the red and blue lines is that near the tube inlet ($z/D = 0.2$ and 5), the no-slip condition at the wall resulted in a significant velocity gradient within the boundary layer and a flat profile at the core for all glycol mixtures regardless of the convection regime. As the fluid flowed further along the tube, the hydrodynamic boundary layer formed along the circumference of the tube and eventually merged. During this process, the velocity profile became parabolic, symmetric, and approached fully developed flow. Beyond this axial position ($z/D = 20$) under forced convection, the velocity profile for all propylene glycol concentrations remained consistent along the tube length, which indicated fully developed hydrodynamic flow.

For mixed convection, beyond an axial position of $z/D = 20$, buoyancy effects began to influence the cross-sectional velocity profile due to the formation of secondary flow within the flow field. This secondary flow led to an asymmetric velocity profile (Fig. 15(b)–(d) and (f)), which is also represented by the contour plots for an axial position of $z/D = 1760$. This explains why the merging position of the hydrodynamic boundary layer shifted downward along the tube length (Fig. 14). However, as the propylene glycol concentration increased, the degree of asymmetry reduced, causing the distance between the peak velocity, indicated by the dotted green line, and the tube centre to decrease. The reduction in asymmetry was due to dampening of secondary flow caused by higher fluid viscosity.

To further investigate these trends, higher propylene glycol concentrations of 70% and 90% were compared at a higher heat flux of 10 kW/m^2 in Fig. 16. A general trend is that for mixed convective flow, the hydrodynamic boundary layer shifted above the centre line of the tube, while the thermal boundary layer shifted below the tube centre line (similar to lower concentrations in Fig. 14). The unexpected upward shift in the hydrodynamic boundary layer position can be attributed to the interplay between the high fluid viscosity and buoyancy forces, such that the fluid viscosity largely supressed the buoyancy effect within the flow along the tube length.

As shown in Fig. 16(a) and (b) the hydrodynamic boundary layer (blue line) merged at the tube centre line, but thereafter the merging point shifted upward along the tube length. This shift was a direct result of the uneven axial velocity distribution (Fig. 16(c) and (d)) which resulted in an increased flow resistance in the lower part of the tube. The uneven velocity distribution resulted from the secondary fluid motion (cooler, denser fluid sunk under the influence of gravity and displaced the less dense, hotter fluid upward). Near the bottom wall, the cooler, denser fluid increased the flow resistance due to its high viscosity, which reduced the axial flow velocity. Conversely, the less viscous and less dense hot fluid had a weaker influence on the axial flow velocity due to weak buoyancy effects. The upper part of the tube retained a higher axial velocity, as shown in the contour plot in Fig. 16(c) and (d), which resulted in an upward shift in asymmetry and consequently, an upward shift in the hydrodynamic boundary layer merging point along the tube length. Hence, the velocity profile became skewed toward the region where the hot fluid naturally rose, with the peak velocity shifting above the centre of the tube.

The red lines in Fig. 16(a) and (b) represents the thermal boundary layer thickness along the tube length. The boundary layer merged at a distance below the tube centre and shifted downward along the tube length. This behaviour can be attributed to the downward shift of the minimum core temperature (Fig. 16(e) and (f)) due to the sinking cooler denser fluid. Near the bottom wall, the cooler denser fluid slowed down the thermal diffusion from the wall due to its low thermal conductivity (Fig. 9), which resulted in slower development of the bottom thermal boundary layer. Hence the thermal boundary layers merged below the tube centre and shifted downward.

5.4. Thermohydraulic behaviour

To investigate the thermohydraulic behaviour of high Prandtl number fluids, the local Nusselt numbers, Colburn *j*-factors, friction factors and *f/j*-factors were compared for different propylene glycol concentrations. Fig. 17(a) and (b) compare the local Nusselt numbers with the theoretical fully developed forced convective Nusselt number of 4.36 (horizontal dotted black line). Furthermore, the solid green line in Fig. 17(a) represents the forced convective correlation of Shah and London [1] for developing flow of the 90% propylene glycol mixture. Near the tube inlet, heat transfer was primarily driven by the steep temperature gradient within the thin thermal boundary layer (Fig. 10) which resulted in high local Nusselt numbers (Fig. 17(a) and (b)), and consequently high Colburn *j*-factors (Fig. 17(c) and (d)). As the fluid flowed along the tube, the thermal boundary layer thickness increased (as seen in Fig. 14) and the local heat transfer from the wall to the fluid decreased resulting in a decrease in the local Nusselt numbers and Colburn *j*-factors. The red arrow in Fig. 17(a) and (b) indicates that the rate of heat transfer in this region increased as the propylene glycol concentration increased. A higher Prandtl number indicates a low

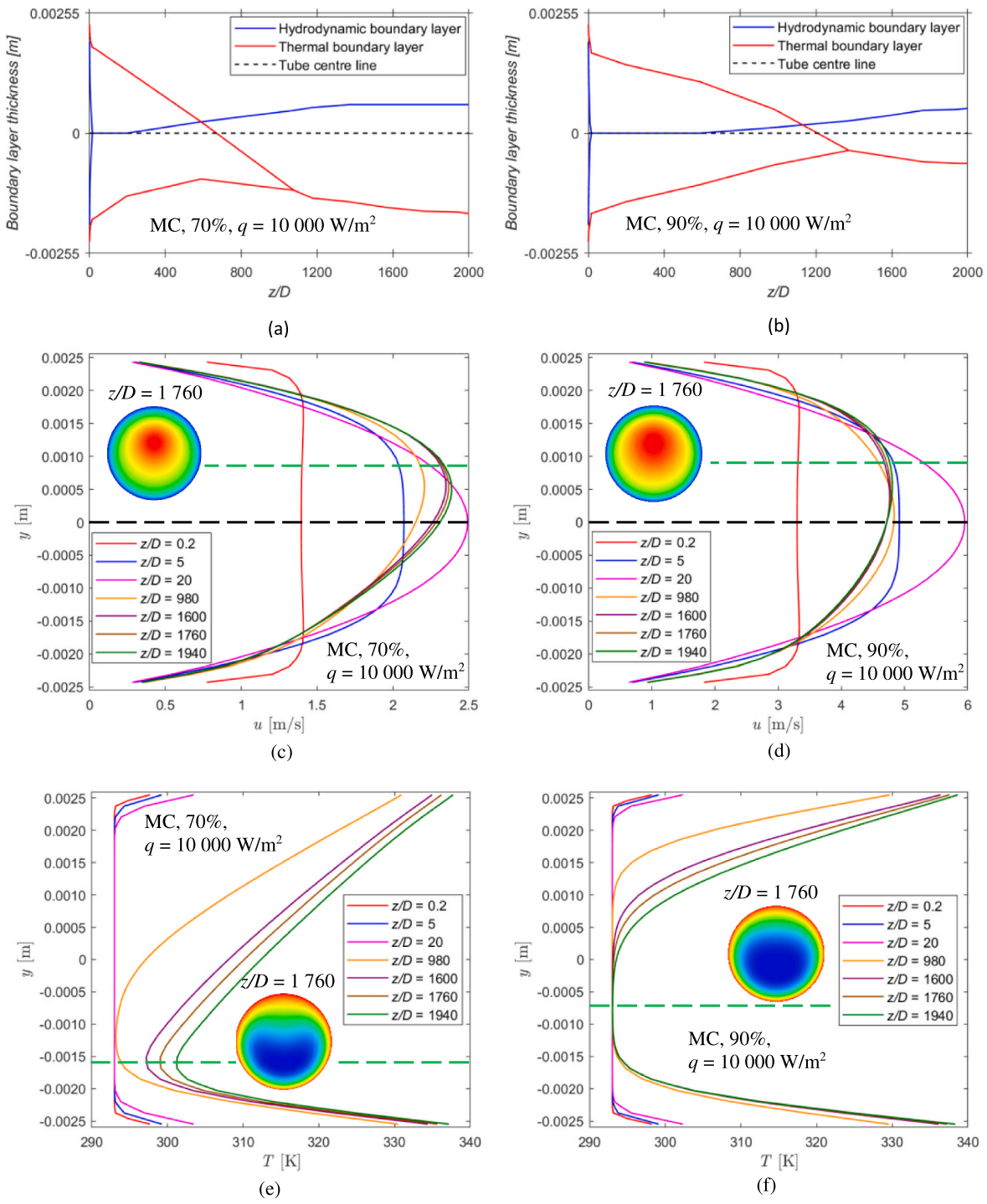

Fig. 16. Comparison of hydrodynamic and thermal boundary layers and cross-sectional velocity and temperature profiles for propylene glycol concentrations of 70% (left column) and 90% (right column) at a Reynolds number of 500 and heat flux of 10 000 W/m^2.

thermal diffusivity which implied that the thermal boundary layer was thinner than the velocity boundary layer and concentrated near the wall due to the higher viscosity. This thinner thermal boundary layer resulted in greater heat transfer as the temperature gradient was steeper near the wall (Fig. 11).

For forced convective heat transfer (Fig. 17(a)), the 0%, 30%, and 50% propylene glycol concentrations became fully developed as evidenced by the Nusselt number converging to the theoretical value of 4.36. However, for higher propylene glycol concentrations of 70%, 80%, and 90% the local Nusselt numbers continued to decrease while their magnitude increased with increasing propylene glycol concentration. Similarly, the Colburn *j*-factors for 0%, 30%, and 50% became nearly constant along the tube length compared to higher concentration of 70%, 80%, and 90% which continuously decreased. As the local Nusselt numbers of the 90% glycol mixture (blue line in Fig. 17(a)) were within 3% of the forced convective correlation of Shah and London [1] (green line), it confirmed that the increase in Nusselt number was due to the flow being developing and not due to mixed convective heat transfer enhancement. As shown in Fig. 15, an increase in the Prandtl number led to a longer thermal entrance region, which is evident by the higher

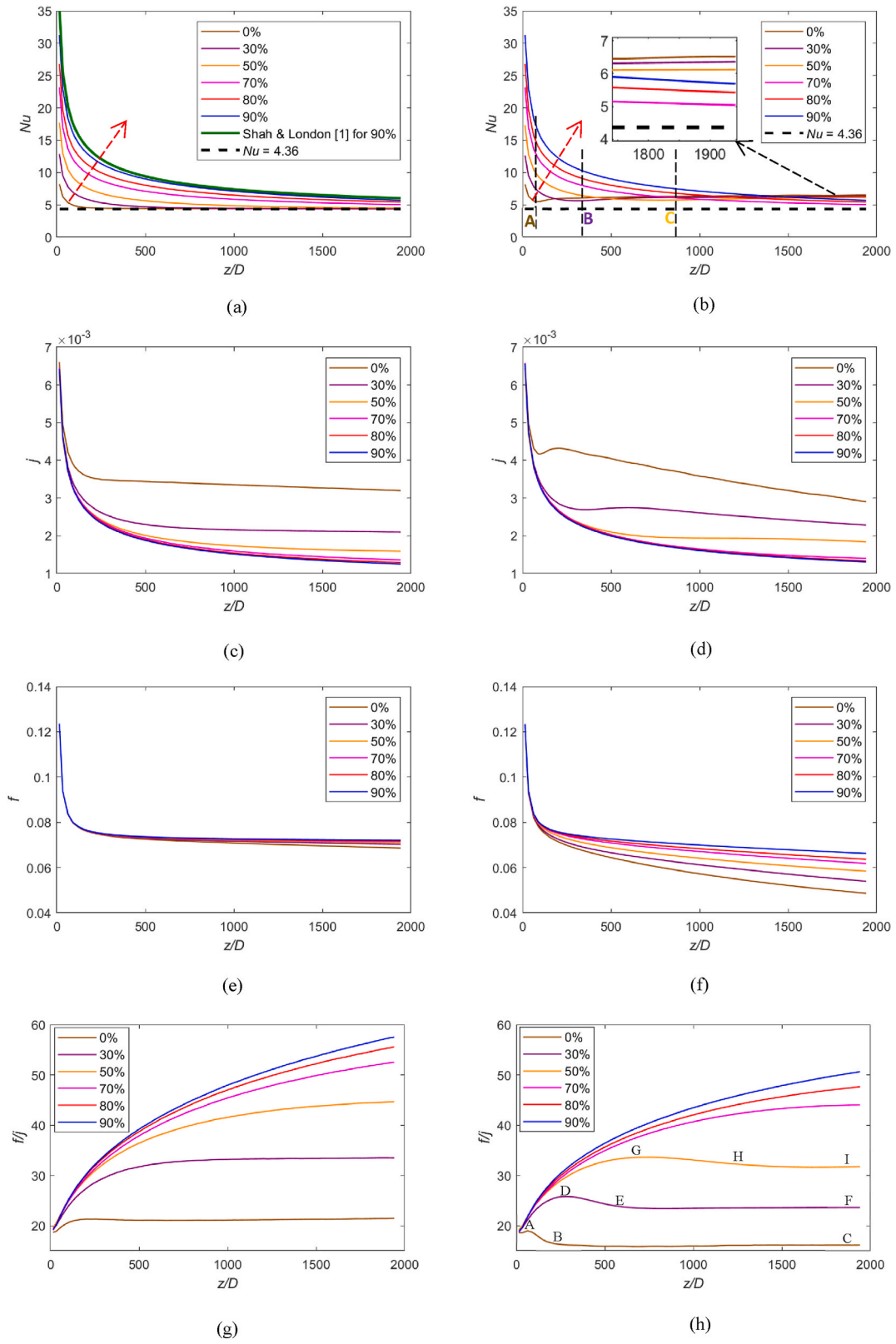

Fig. 17. Comparison of (a–b) local Nusselt numbers, (c–d) local Colburn *j*-factors, (e–f) local friction factors, and (g–h) *f*/*j*-factors at a Reynolds number of 500 for heat fluxes of 200 W/m^2 (forced convection, left column) and 2000 W/m^2 (mixed convection, right column).

temperature gradient at the wall (Fig. 8).

For mixed convective flow, the buoyancy force (Fig. 12) increased as the thermal boundary layer thickness developed from the tube inlet. Points A, B, and C, corresponding to axial positions of $z/D = 92$, 409, and 925, respectively, in Fig. 17(b) indicate the axial positions at which buoyancy-induced secondary flow was sufficient to cause an increase in local Nusselt number for 0%, 30%, and 50% propylene glycol concentrations, respectively. The thermal boundary layer of higher propylene

glycol concentrations developed slower due to the lower buoyancy effects and thermal conductivities. Therefore, the axial position at which buoyancy effects became significant (points A to C), increased with increasing propylene glycol concentration. Furthermore, an increase in viscosity dampened buoyancy effects (Figs. 10 and 13), which explains why the Nusselt numbers decreased with increasing propylene glycol concentration. Hence, near the tube outlet where buoyancy effects became a significant mechanism for heat transfer, a distinct crossover occurred. The local Nusselt number for 0%, 30% and 50% propylene glycol concentrations surpassed that of the 90% glycol concentration by 14.5%, 7.5%, and 4.1%, respectively, as well as the forced convective values by 40%, 28%, and 15% respectively.

In Fig. 17(d), the downward slope of the local Colburn *j*-factors reflects the interplay between heat transfer enhancement caused by buoyancy effects and changes in fluid properties due to the increasing fluid temperature along the tube length. Although the enhanced mixing due to buoyancy-induced secondary flow caused the local Nusselt numbers to increase in Fig. 17(b), the Colburn *j*-factors decreased due to the fluid's decreasing viscosity and Prandtl number. This trend became less prominent with increasing propylene glycol concentration due to the decreasing temperature gradient along the tube length caused by the combined effect of high fluid viscosity and low thermal conductivity.

To relate the effect of high Prandtl numbers on the pumping power, Fig. 17(e) and (f) compare the forced and mixed convective local friction factors of the different propylene glycol concentrations. Near the tube inlet, where the fluid is hydrodynamically developing, the local friction factors in both forced and mixed convective flows were a maximum and decreased sharply. This was due to the higher flow resistance caused by the steep velocity gradient near the wall and the uniform velocity profile at the core (Fig. 15). As the fluid was heated along the tube length, the viscosity decreased (Fig. 9), which led to a reduction in wall shear stress and gradual decline in the local friction factor. This effect became more pronounced in mixed convective flow because the buoyancy effects led to greater variation in viscosity. The viscosity of 0%, 30%, 50%, 70%, 80%, and 90% concentrations decreased by 57%, 41%, 29%, 19%, 3% and 2.5%, respectively, compared to forced convective flow which decreased by 10%, 5%, 3%, 2%, 1.5%, and 1%, respectively. Consequently, the local mixed convective friction factors were lower than forced convective flow. As expected, the local friction factors increased with increasing propylene glycol concentration due to the increased viscosity. Hence, the local friction factor for the 90% propylene glycol concentration was on average 2% and 18% higher than for forced and mixed convective flow of pure water (0% propylene glycol), respectively.

The trade-off between pumping power and heat transfer enhancement in the form of f/j-factors is depicted in Fig. 17(g) and (h), with lower values being more favourable. In forced convective flow (Fig. 17(g)), the f/j-factors increased from the tube inlet towards the outlet. This indicates that the heat transfer performance decreased due to the thickening of the thermal boundary layer along the tube length (Fig. 14). For mixed convective flow (Fig. 17(h)), a different trend was observed for lower propylene glycol concentrations (0%, 30%, and 50%). Similar to the forced convective flow, it increased from the inlet as the thermal boundary layer developed, to a peak (Points A, D, and G), decreased to a minimum (Points B, E and H) due to buoyancy effects which reduced the boundary layer thickness, enhancing heat transfer performance, thereafter nearly becaming constant. However, for higher propylene glycol concentrations (70%, 80% and 90%), it increased continuously due to the high fluid viscosity dampening buoyancy effects. Fig. 17(g) and (h) indicate that it is more favourable for heat exchangers to operate with mixed convective flow.

6. Conclusions

This study critically investigated the influence of Prandtl number on the thermohydraulic behaviour of laminar mixed convective flow through horizontal tubes heated at a constant heat flux. Different propylene glycol concentrations (0%, 30%, 50%, 70%, 80%, and 90%) were considered for heat fluxes of 200-10 000 W/m^2 and Reynolds numbers of 250-2000. The forced convective analysis revealed that for increased propylene glycol concentrations, the wall-fluid temperature difference increased, and heat transfer was confined to the thermal boundary layer near the tube wall. Although the Nusselt numbers increased with increasing Prandtl number, the increase was not due to enhanced mixing, rather due to a thinner thermal boundary layer and an increased temperature gradient. Furthermore, this did not lead to increased thermal performance as higher propylene glycol concentrations also had greater flow resistance (higher local friction factors). It was found that an increase in Prandtl number increased the forced convective thermal entrance length but decreased the hydrodynamic entrance length. This was because an increase in viscosity resulted in stronger momentum diffusion, which supported faster hydrodynamic boundary layer growth.

The mixed convective results provided valuable insights into the interplay between buoyancy and viscosity effects. Although the buoyancy force was found to increase for 70%, 80%, and 90% concentrations (thus with increasing Prandtl number) by approximately 67%, 72% and 74% compared to the 0% glycol concentration, the actual buoyancy effects decreased by up to 95% due to the increased viscosity that dampened secondary flow. An increase in buoyancy force increased the vorticity magnitude and circulation strength, but these effects were confined near the tube wall due to the high fluid viscosity which prevented redistribution into the core of the flow, resulting in lower secondary flow strengths. When buoyancy effects were quantified using the secondary flow strength, three distinct regions were identified: (1) developing region, (2) suppression region, and (3) enhancement region. As the Prandtl number increased, the local Nusselt numbers near the inlet of the tube increased, due to the thinner thermal boundary layer, while the local Nusselt numbers downstream of the tube decreased because the buoyancy-induced secondary flow that enhanced mixing and heat transfer was suppressed. Hence the local Nusselt number for 0%, 30%, and 50% concentrations surpassed the 90% glycol concentration by 14.5%, 7.5%, and 4.1%, respectively.

The development of the mixed convective hydrodynamic boundary layer varied for lower Prandtl numbers, where buoyancy effects dominated, and higher Prandtl numbers, where viscous effects dominated. When viscous effects dominated, the velocity profile skewed above the tube's centre line, unlike in fluids with lower Prandtl numbers, and the merging point of the hydrodynamic boundary layer shifted upward along the tube length. For all Prandtl numbers, the mixed convective thermal boundary layer merged below the centre line and the merging point continued to move downwards along the tube until the flow became fully developed. As the Prandtl number increased, mixed convective flow was dampened and the merging position moved towards the centre line and further downstream, indicating a longer thermal entrance length.

The overall thermohydraulic performance revealed that mixed convective conditions are indeed more favourable for heat exchangers to operate in when using high Prandtl number heat transfer fluids. An increase in buoyancy effects not only increased the heat transfer coefficients but also decreased the friction factors due to lower viscosities and enhanced mixing. An improved fundamental understanding of enhancing mixed convective flow for high Prandtl number fluids is valuable to improve the energy efficiency of thermal management solutions by tailoring it based on different viscous heat transfer fluids.

CRediT authorship contribution statement

Marilize Everts: Writing – review & editing, Supervision, Resources, Project administration, Conceptualization. **Oluwasegun S. Omosehin:** Writing – original draft, Visualization, Validation, Methodology, Investigation, Formal analysis, Data curation. **Wilhelm J. van den Bergh:** Writing – review & editing, Supervision, Resources.

Declaration of competing interest

The authors declare that they have no known competing financial interests or personal relationships that could have appeared to influence the work reported in this paper.

Acknowledgements

The authors duly appreciate and acknowledge the resources provided by the University of Pretoria as well as the Centre for High-Performance Computing (CHPC) in Cape Town, South Africa, which made the numerical simulations possible.

Data availability

Data will be made available on request.

References

[1] R.K. Shah, Laminar Flow Forced Convection in Ducts, Academic press, New York, 1978.
[2] R. Siegel, E. Sparrow, T. Hallman, Steady laminar heat transfer in a circular tube with prescribed wall heat flux, Applied Scientific Research, Section A 7 (1958) 386–392.
[3] S.W. Churchill, H. Ozoe, Correlations for laminar forced convection with uniform heating in flow over a plate and in developing and fully developed flow in a tube, J. Heat Tran. 95 (1) (1973) 78–84, https://doi.org/10.1115/1.3450009.
[4] R. Martínez Cuenca, R. Mondragón, L. Hernández, C. Segarra, J.C. Jarque, T. Hibiki, J.E. Juliá, Forced-convective heat-transfer coefficient and pressure drop of water-based nanofluids in a horizontal pipe, Appl. Therm. Eng. 98 (2016) 841–849, https://doi.org/10.1016/j.applthermaleng.2015.11.050.
[5] M. Everts, M. Mahdavi, J.P. Meyer, M. Sharifpur, Development of the hydrodynamic and thermal boundary layers of forced convective laminar flow through a horizontal tube with a constant heat flux, Int. J. Therm. Sci. 186 (2023), https://doi.org/10.1016/j.ijthermalsci.2022.108098.
[6] M. Yasuo, F. Kozo, T. Shinobu, N. Masakuni, Forced convective heat transfer in uniformly heated horizontal tubes 1st report—Experimental study on the effect of buoyancy, Int. J. Heat Mass Tran. 9 (5) (1966) 453–463.
[7] S.T. McComas, E.R.G. Eckert, Combined free and forced convection in a horizontal circular tube, J. Heat Tran. 88 (2) (1966) 147–152, https://doi.org/10.1115/1.3691494.
[8] A. Bergles, R. Simonds, Combined forced and free convection for laminar flow in horizontal tubes with uniform heat flux, Int. J. Heat Mass Tran. 14 (12) (1971) 1989–2000.
[9] H.A. Mohammed, Y.K. Salman, Combined natural and forced convection heat transfer for assisting thermally developing flow in a uniformly heated vertical circular cylinder, Int. Commun. Heat Mass Tran. 34 (4) (2007) 474–491, https://doi.org/10.1016/j.icheatmasstransfer.2007.01.001.
[10] G.S. Barozzi, E. Zanchini, M. Mariotti, Experimental investigation of combined forced and free convection in horizontal and inclined tubes, Meccanica 20 (1985) 18–27.
[11] J. P. Meyer, A. I. Bashir, and M. Everts, "Single-phase mixed convective heat transfer and pressure drop in the laminar and transitional flow regimes in smooth inclined tubes heated at a constant heat flux," Exp. Therm. Fluid Sci., vol. 109, doi: 10.1016/j.expthermflusci.2019.109890.
[12] J.P. Meyer, M. Everts, Single-phase mixed convection of developing and fully developed flow in smooth horizontal circular tubes in the laminar and transitional flow regimes, Int. J. Heat Mass Tran. 117 (2018) 1251–1273, https://doi.org/10.1016/j.ijheatmasstransfer.2017.10.070.
[13] M. Everts, M. Mahdavi, M. Sharifpur, J.P. Meyer, Simultaneous development of the hydrodynamic and thermal boundary layers of mixed convective laminar flow through a horizontal tube with a constant heat flux, Int. J. Therm. Sci. 187 (2023), https://doi.org/10.1016/j.ijthermalsci.2023.108178.
[14] Q. Chen, N. Harris, K.J. Craig, M. Everts, Mixed convective laminar flow through non-circular channels heated at a constant heat flux, Int. J. Therm. Sci. 210 (2025), https://doi.org/10.1016/j.ijthermalsci.2024.109664.
[15] Z. Daotong, L. Jiping, Z. Qingfu, Numerical simulations of 3d-flow for Laminar mixed convection in horizontal rectangular tubes, J. Eng. Thermophys. 1 (2009) 141–143.
[16] R. Ben Mansour, N. Galanis, C.T. Nguyen, Developing laminar mixed convection of nanofluids in an inclined tube with uniform wall heat flux, Int. J. Numer. Methods Heat Fluid Flow 19 (2) (2009) 146–164, https://doi.org/10.1108/09615530910930946.
[17] M. Akbari, A. Behzadmehr, F. Shahraki, Fully developed mixed convection in horizontal and inclined tubes with uniform heat flux using nanofluid, Int. J. Heat Fluid Flow 29 (2) (2008) 545–556, https://doi.org/10.1016/j.ijheatfluidflow.2007.11.006.
[18] R. Ben Mansour, N. Galanis, C.T. Nguyen, Experimental study of mixed convection with water–Al2O3 nanofluid in inclined tube with uniform wall heat flux, Int. J. Therm. Sci. 50 (3) (2011) 403–410, https://doi.org/10.1016/j.ijthermalsci.2010.03.016.
[19] L. Colla, L. Fedele, M.H. Buschmann, Laminar mixed convection of TiO2–water nanofluid in horizontal uniformly heated pipe flow, Int. J. Therm. Sci. 97 (2015) 26–40, https://doi.org/10.1016/j.ijthermalsci.2015.06.013.
[20] J. Buongiorno, Convective transport in nanofluids, J. Heat Tran. 128 (3) (2005) 240–250, https://doi.org/10.1115/1.2150834.
[21] C. Yang, W. Li, Y. Sano, M. Mochizuki, A. Nakayama, On the anomalous convective heat transfer enhancement in nanofluids: a theoretical answer to the nanofluids controversy, J. Heat Tran. 135 (5) (2013), https://doi.org/10.1115/1.4023539.
[22] M. Wang, T. Tsuji, Y. Nagano, Mixed convection with flow reversal in the thermal entrance region of horizontal and vertical pipes, Int. J. Heat Mass Tran. 37 (15) (1994) 2305–2319.
[23] S. Zhang, Mixed convective heat transfer of medium-prandtl-number fluids in horizontal circular tubes, Int. J. Heat Mass Tran. 190 (2022), https://doi.org/10.1016/j.ijheatmasstransfer.2022.122740.
[24] K. Cheng, S. Hong, G. Hwang, Buoyancy effects on laminar heat transfer in the thermal entrance region of horizontal rectangular channels with uniform wall heat flux for large Prandtl number fluid, Int. J. Heat Mass Tran. 15 (10) (1972) 1819–1836.
[25] M.-S. Chae, B.-J. Chung, Laminar mixed-convection experiments in horizontal pipes and derivation of a semi-empirical buoyancy coefficient, Int. J. Therm. Sci. 84 (2014) 335–346, https://doi.org/10.1016/j.ijthermalsci.2014.06.007.
[26] F.C. Chou, G.J. Hwang, Vorticity-velocity method for the Graetz problem and the effect of natural convection in a horizontal rectangular channel with uniform wall heat Flux, J. Heat Tran. 109 (3) (1987) 704–710, https://doi.org/10.1115/1.3248145.
[27] Z.-Z. Feng, W. Li, Laminar mixed convection of large-prandtl-number in-tube nanofluid flow, Part I: experimental study, Int. J. Heat Mass Tran. 65 (2013) 919–927, https://doi.org/10.1016/j.ijheatmasstransfer.2013.07.005.
[28] ASHRAE Handbook Heating Ventilating and air-conditioning Applications, [S.L.], American society of heating refrigerating and air-conditioning engineers Inc. (ASHRAE), 2019.
[29] M. Everts, J.P. Meyer, Flow regime maps for smooth horizontal tubes at a constant heat flux, Int. J. Heat Mass Tran. 117 (2018) 1274–1290, https://doi.org/10.1016/j.ijheatmasstransfer.2017.10.073.
[30] M. Everts, J.P. Meyer, Heat transfer of developing and fully developed flow in smooth horizontal tubes in the transitional flow regime, Int. J. Heat Mass Tran. 117 (2018) 1331–1351, https://doi.org/10.1016/j.ijheatmasstransfer.2017.10.071.